University of Alberta

Spatial Modeling of the Composting Process

by

Anastasia Lukyanova

A thesis submitted to the Faculty of Graduate Studies and Research
in partial fulfillment of the requirements for the degree of

Master of Science

Department of Mathematical and Statistical Sciences

Department of Civil and Environmental Engineering

Spring 2012
Edmonton, Alberta

Abstract

Spatial heterogeneity is an important characteristic of large-scale composting, however, only a few spatial models for composting exist to date. In this thesis, a novel spatial model for composting is developed. The model is applicable for any one-, two-, or three-dimensional pile geometry. It accounts for the consumption of organic matter and therefore considers the whole composting process from the beginning to the end of decomposition, gives a realistic prediction of the buoyant air flow patterns, incorporates the cooling by passing air, and includes the effects of compaction. The model is validated using existing data from a series of in-vessel composting experiments, and then utilized to simulate windrow composting. Effects of the windrow size variation are explored and it is demonstrated that decomposition speed increases as the pile height increases, however, for large piles this increase becomes smaller as oxygen concentration limitations become significant. Air floor technology is simulated, demonstrating a significant decrease in decomposition time even for passive aeration. The developed model can be a useful tool in process optimization and facility design.

Acknowledgments

I would like to acknowledge the Pacific Institute for Mathematical Sciences (PIMS) for providing funding for this thesis through the International Graduate Training Center Program (IGTC).

There are many individuals who played an important role in my M.Sc. adventure. First, I thank my supervisor Dr. Gerda de Vries, who supported me throughout my program. An excellent supervisor, she provided me with the freedom to explore this new area of research. Her encouragement and faith in the project were a constant source of inspiration. I thank my co-supervisor Dr. Daryl McCartney for his enthusiasm and support. His extensive experience and insight into the field were invaluable in helping me find my way through the world of composting science. I thank Dr. Shouhai Yu for providing the data for the project and for always finding time to answer my questions.

I am grateful to all the members of the compost team: Dr. Gerda de Vries, Dr. Morris Flynn, Dr. Jerry Leonard, Dr. Shouhai Yu, and Mark Roes. Our meetings provided me with constant constructive feedback and inflow of ideas. Without their input, this project could not have come to fruition. I also thank Dr. Peter Minev for his helpful advice and expertise with numerical aspects of our work. I am grateful to Ulrike Schlaegel for her supportive friendship and advice. A special thank you goes to Noland Germain for his loving reassurance and encouragement.

Anastasia Lukyanova

Contents

List of Tables

List of Figures

1 Introduction

Composting is an environmentally sustainable way of managing organic waste that has been used since ancient times. It is commonly defined as decomposition of organic matter by microorganisms under aerobic conditions. Composting is the natural way to recycle nutrients back into the soil. Bacteria and other microorganisms consume organic matter and oxygen to stabilize the organics and produce compost. The final product is rich in nutrients that are beneficial for plants and can be used as a soil amendment. The main products of the biological decomposition are carbon dioxide, water, and heat (see Figure 1.1).

Even though composting has been utilized for so long, it still remains an art rather than a science due to the high complexity of the process [Gajalakshmi and Abbasi, 2008]. Mathematical models for composting are developed to better understand, predict, facilitate, and optimize the composting process. Mathematical models for composting have appeared in the literature since 1976 [Mason, 2006]. Most of the models developed to date are for in-vessel composting and, although providing valuable insights into the composting process, these models are unsuitable for simulating industrial composting. In addition, the majority of existing models are spatially uniform [Mason, 2006], which is a reasonable simplification for modeling in-vessel composting under controlled conditions. However, modern composting facilities most often employ windrow technology [Gajalakshmi and Abbasi, 2008]. Windrow technology is a method of producing compost by piling

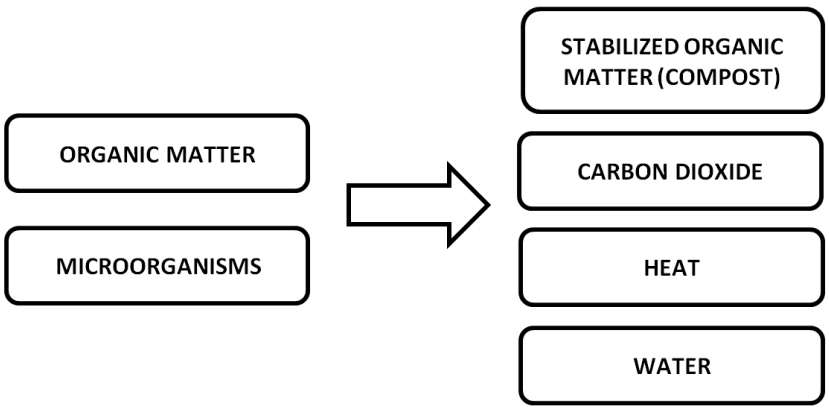

Figure 1.1: Composting diagram.

Figure 1.2: Compost windrows at the Bear Path Farm in Whately, Massachusetts. Source: `http://www.bearpathfarm.com/how_BPF_makes_compost.html`. Last accessed on September 15, 2011.

the composting material in long rows which are called windrows (see Figure 1.2). In a windrow, temperature, oxygen concentration, and moisture profiles can become highly inhomogeneous, which makes considering average measurements impossible, and thus requires a spatial model. Therefore, spatial models of composting are chosen as the focus of our work.

In Section 1.1, we give an overview of the thesis structure and give a brief description of each of the chapters. In Section 1.2, we describe the basic terms and laws that will be used in the development of our model. We discuss the concepts of porous media, air-filled porosity, permeability, and derive Darcy's Law with buoyancy.

1.1 Thesis overview

In Chapter 2, we begin by discussing the existing spatial models for composting that served as a starting point for our work. We consider models by Finger et al. [1976], Sidhu et al. [2007b], Sidhu et al. [2007a], Luangwilai et al. [2010], and Luangwilai and Sidhu [2011]. We discuss the strengths and shortcomings of each of the models, therefore setting up the foundation and providing motivation for our work. We demonstrate that these models do not provide a realistic prediction of the buoyant air flow pattern in the compost pile and neglect the consumption of organic matter, therefore considering only the high-rate stage of composting. Most models neglect the cooling of the compost by

passing air, and the models that do account for it use a prescribed, simplified air flow pattern.

In Chapter 3, we develop a new spatial model for composting which overcomes the limitations of the existing models. The model is applicable for any pile geometry, one-, two-, or three-dimensional; it gives a realistic prediction of the buoyant flow of air through the pile; incorporates the consumption of organic matter and examines the process from the beginning to the end of decomposition; and includes the cooling of the compost by passing air. The model also includes the effects of compaction by considering some of the model parameters to be dependent on the depth.

In Chapter 4, the model is validated against the experimental data from Yu [2007]. The data set was obtained from a series of in-vessel composting experiments conducted in laboratory conditions. We fix the parameters that have well-established values in the literature and vary the parameters that have a wide range of reported values to obtain good agreement between the model's predictions and the experimental data. Therefore, a parameter set for windrow simulations is obtained.

In Chapter 5, we focus on modeling windrow composting. We consider a two-dimensional cross-section of a windrow, and discuss the model's predictions of the temperature, oxygen concentration, substrate availability, and pressure profiles. The model gives a detailed prediction of the air flow patterns in a windrow, which are not simulated by the existing models. The effects of varying the height of the windrow on composting process are investigated. We demonstrate that efficiency increases as the pile height increases, however, for large piles this increase becomes smaller as oxygen limitations come into play. We show how the developed model can be used to simulate aerated windrows. The model's predictions suggest that even passive aeration can significantly decrease the time required for decomposition.

Finally, in Chapter 6, we present the conclusions and discuss recommendations for future work.

1.2 Introduction to Terminology

In this section, we introduce the basic terms and laws necessary to understand mathematical and numerical modeling of the composting process. We discuss the concepts of porous media, porosity, permeability, and introduce Darcy's Law.

1.2.1 Porous Media and Porosity

Porous medium is simply a material that has void spaces. Many natural and man-made materials can be considered as porous media: soil, rock, sand, filters and membranes, coal, etc. The void space of the material can be filled with a fluid, e.g., water, air, or oil. Porous medium is often characterized by its porosity, which is the relation between the volume of the void space V_v and the total volume V:

$$\Phi = \frac{|V_v|}{|V|}. \tag{1.1}$$

Porosity may vary from one part of the material to another, and can be considered as a point function [Fulks et al., 1971]:

$$\Phi(\vec{x}) = \lim_{|V|\to 0} \frac{|V_v|}{|V|}. \tag{1.2}$$

In this thesis, we will be focusing on the flow of air through the composting material, which is a porous medium. Thus, we will use the concept of air-filled porosity (AFP), which is the fraction of the void space in compost that is filled with air (see Figure 1.3):

$$\Phi = \lim_{|V|\to 0} \frac{|V_{air}|}{|V|}. \tag{1.3}$$

The air-filled porosity is also referred to in the literature as free air space (FAS).

1.2.2 Darcy's Law and Permeability

In order to describe the flow of fluids through porous media, Darcy's Law is widely used. Darcy's Law connects the flow rate through porous media with the pressure gradient.

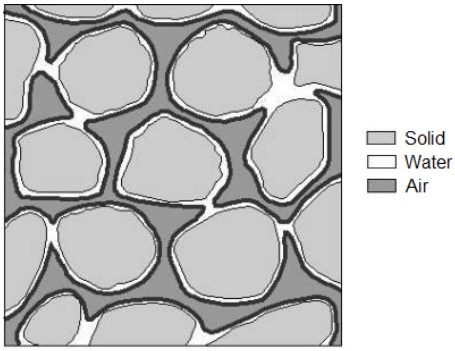

Figure 1.3: Porous medium diagram for composting.

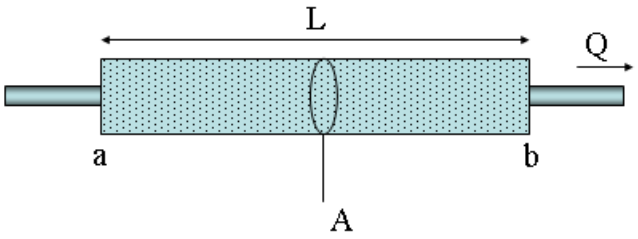

Figure 1.4: Darcy's Law diagram. Source: `http://en.wikipedia.org/wiki/Darcy's_law`. Last accessed on September 16, 2011.

The law was derived empirically by Henry Darcy in 1856 based on his experiments with water flowing through a sand filter [Brown et al., 2003]. The basic form of Darcy's Law is as follows:

$$Q = -\frac{kA}{\mu}\frac{P_b - P_a}{L}, \tag{1.4}$$

where Q (m^3/s) is the total discharge, k (m^2) is the permeability, A (m^2) is the cross-sectional area, $(P_b - P_a)$ (Pa) is the pressure difference between locations b and a, L (m) is the length, and μ $(Pa \cdot s)$ is the viscosity of the fluid (see Figure 1.4). Permeability k characterizes how easily a fluid can penetrate the porous medium. Although related to the porosity value, in general, it is not determined by it. Permeability depends on the structure of the pore space and on how connected the pores are. Two materials with the same porosity values can have very different values of permeability.

Darcy's Law can be written in the following more general form:

$$\vec{q} = -\frac{k}{\mu}\nabla P, \tag{1.5}$$

where $\vec{q}\ (m/s)$ is the volume flux (discharge per unit area). It should be noted that for flows in porous media, the volume flux $\vec{q}$ is not equal to the interstitial velocity of the fluid $\vec{v}$. The velocity $\vec{v}$ is the speed at which the fluid is traveling through the pores of the material. Not all the volume of the material is available to the fluid, and thus the velocity $\vec{v}$ and the volume flux $\vec{q}$ are related by the following expression [Fulks et al., 1971]:

$$\vec{q} = \Phi\vec{v}. \tag{1.6}$$

The volume flux of the fluid $\vec{q}$ is always smaller than the fluid velocity in the pores of the porous medium matrix $\vec{v}$.

We are interested in describing the buoyant flow of air through compost, therefore Darcy's Law (1.5) needs to be extended to include buoyancy. The derivation presented here has been modified from Yu et al. [2008]. Buoyant flow of air occurs as a result of heating inside the compost pile. As the air heats and expands, it becomes lighter than the ambient air. Let V_{amb} be a small volume of air at an ambient temperature T_{amb}. Once heated to a temperature T, the air will expand and occupy a volume V, where $V > V_{amb}$. We assume that the pressure of air is relatively constant throughout the pile and apply the ideal gas law to obtain the following relationship:

$$\frac{V}{V_{amb}} = \frac{T}{T_{amb}}. \tag{1.7}$$

According to Archimedes' principle, the buoyant force applied to the heated air is equal to the weight of ambient air in the expanded volume V:

$$F_{buoyancy} = C_{air}^{amb} gV, \tag{1.8}$$

where $C_{air}^{amb}\ (kg/m_{air}^3)$ is the ambient air density, and $g\ (m/s^2)$ is the gravitational acceleration. The heated air is also affected by gravity, and the force due to gravity is

$$F_{gravity} = C_{air}^{amb} gV_{amb}. \tag{1.9}$$

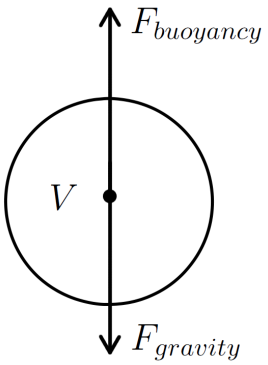

Figure 1.5: Force diagram.

The resulting force is equal to the difference between the buoyant force $F_{buoyancy}$ and the gravity force $F_{gravity}$ (see Figure 1.5):

$$F_{total} = F_{buoyancy} - F_{gravity} = C_{air}^{amb} g(V - V_{amb}), \tag{1.10}$$

which can be rewritten using (1.7) as

$$F_{total} = C_{air}^{amb} gV(1 - \frac{T_{amb}}{T}). \tag{1.11}$$

The force per unit volume then is

$$F_{total}^{0} = C_{air}^{amb} g(1 - \frac{T_{amb}}{T}). \tag{1.12}$$

We have divided the total force by the volume V to obtain the same units as the pressure gradient ∇P, so that we can include it into Darcy's Law (1.5). If we consider V to be a small volume of the porous medium, it will contain $\Phi \cdot V$ volume of air. Therefore, Darcy's Law with buoyancy can be written as

$$\vec{q} = -\frac{k}{\mu}(\nabla P - C_{air}^{amb} g\Phi(1 - \frac{T_{amb}}{T})\vec{e_z}), \tag{1.13}$$

where $\vec{e_z}$ is a unit vector pointing upwards. We can see that if $T > T_{amb}$ the air will be forced upwards in the direction $\vec{e_z}$, and if $T < T_{amb}$ the air will move down. We will later use the expression (1.13) in the derivation of our model (see Section 3.3).

2 A Review of the Existing Spatial Models

In this chapter, we discuss the existing spatial models for composting developed by Finger et al. [1976], Sidhu et al. [2007a], Sidhu et al. [2007b], Luangwilai et al. [2010], and Luangwilai and Sidhu [2011], as these models have formed the starting basis for our research. The description of each of the models is followed by a brief summary section where we discuss the model's strengths and shortcomings.

2.1 Model by Finger

In 1976, Finger et al. [1976] formulated a spatial model that predicts temperature and oxygen concentration profiles of a compost windrow. This model was the first mathematical model of composting to appear in the literature [Mason, 2006]. Finger's model can be used for one-, two-, or three-dimensional geometries, and looks at the steady-state profiles of temperature and oxygen which correspond to the thermophilic, or high-rate stage of composting. The model by Finger is a reaction-diffusion system of two equations:

$$\frac{\partial T}{\partial t} = D_T \Delta T + K_T \exp\left(-\frac{E_a}{RT}\right) C^*, \tag{2.1}$$

$$\frac{\partial C^*}{\partial t} = D_0 \Delta C^* - K_0 \exp\left(-\frac{E_a}{RT}\right) C^*, \tag{2.2}$$

where T (K) is the temperature, C^* $(g/liter)$ is the oxygen concentration, D_T (ft^2/hr) is the thermal diffusivity of the compost, D_0 (ft^2/hr) is the oxygen diffusivity, K_T (K/hr) is the heat release rate, K_0 $(1/hr)$ is the rate of oxygen consumption, and t (hr) is the time. In the equation for temperature, (2.1), the first term on the right-hand side represents the diffusion of heat through the compost pile, and the second term stands for the heat released by the microorganisms. In the equation for the oxygen concentration, (2.2), the first term on the right-hand side represents molecular diffusion of oxygen, and the second term corresponds to the consumption of oxygen by the microorganisms. Organic matter is assumed to be abundant and therefore is not included in the model.

Finger uses Arrhenius equation to describe how the reaction rate depends on the

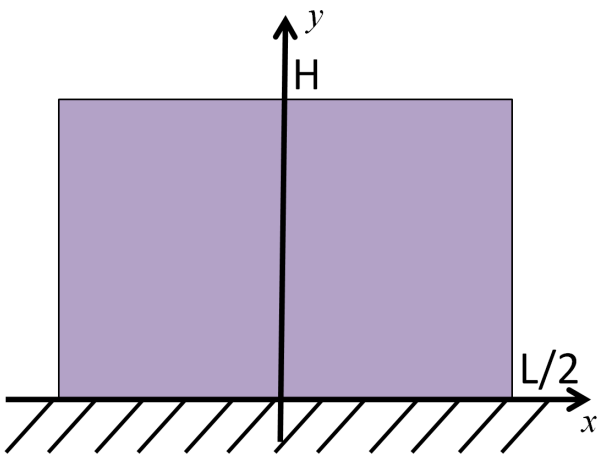

Figure 2.1: The pile geometry chosen by Finger et al. [1976].

temperature. Arrhenius equation is a widely used formula describing how the rate of a chemical reaction depends on the temperature. The general form of the Arrhenius equation is as follows:

$$k = A \exp\left(-\frac{E_a}{RT}\right), \tag{2.3}$$

where k $(1/s)$ is the reaction rate, A $(1/s)$ is the pre-exponential factor, E_a (cal/mol) is the activation energy, and R $(cal/K\text{-}mol)$ is the gas constant. The value of the activation energy used by Finger is $1.11 \cdot 10^4$ cal/mol.

The model by Finger sets the reaction rate proportional to the oxygen concentration (see second terms on the right-hand side of the equations (2.1) and (2.2)). This proportionality is derived from the assumption that the rate of biological oxidation is equal to the rate of oxygen transfer from the gas phase of the compost matrix into the liquid and solid phases. The details of this derivation can be found in the original paper [Finger et al., 1976].

The authors consider a two-dimensional rectangular cross-section of a compost pile shown in Figure 2.1. Due to the symmetry, half of this cross-section is chosen as the model domain:

$$0 \leq x \leq L/2, \quad 0 \leq y \leq H. \tag{2.4}$$

The initial temperature and oxygen concentrations in the pile are assumed to be ambient (the ambient temperature is 300 K, and the ambient oxygen concentration is 21%).

The oxygen concentration and temperature on the top and on the sides of the pile are maintained as ambient. There is no flux for temperature or oxygen along the center line by symmetry. There is no oxygen flux on the bottom; however, there is heat flux. It is assumed that the heat dissipates into the ground and that the temperature decreases linearly until it reaches the ambient temperature value a few feet below the ground.

The number values for the parameters are determined by fitting the model to experimental data. The four parameters K_T, D_T, K_0, and D_0 are found to have the following values:

$$K_T = 2.38 \times 10^{-10}\ K/hr, \tag{2.5}$$

$$D_T = 6.86 \times 10^{-12}\ ft^2/hr, \tag{2.6}$$

$$K_0 = 3.31 \times 10^{6}\ 1/hr, \tag{2.7}$$

$$D_0 = 6.93 \times 10^{-7}\ ft^2/hr. \tag{2.8}$$

It should be noted that model equation (2.1) is dimensionally inconsistent if the oxygen concentration is measured in $g/liter$, as the authors state in the variable list. However, in the numerical simulations the oxygen concentration is plotted in %, which is probably the units it should have in equation (2.1).

2.1.1 Applied Studies Based on the Model

Finally, the model is utilized to predict the effects of varying parameters such as external temperature, size of the pile, substrate density, and insulating the bottom of the pile on the composting process. The different options are compared based on the reaction rate and its uniformity along the center line (y axis) of the pile. Ideally, according to the authors, the substrate would be converted uniformly and at a high rate. Here we briefly list some of the studies carried out by the authors:

- *The Insulation Study* investigated the effects of thermally insulating the bottom of the compost pile. It was concluded that the insulation resulted in an increase in the degradation rate without any significant loss in the rate uniformity.

- *The External Temperature Study* compared the degradation rates for 300 K and 320 K ambient temperatures. It was found that the increase in temperature caused the reaction rate to increase in the top portion of the pile but to decrease in the interior. Thus, according to the model, the substrate was being converted non-uniformly at a higher temperature.

- *The Size Study* varied the height of the pile while keeping its relative shape constant. Three different values for the height of the pile were considered: 5, 8, and 11 ft. The corresponding widths were 5.4, 8.5, and 11.8 ft, respectively. The model showed that the 8-foot pile was optimal in terms of the rate of biological degradation and its uniformity.

- *The Density Study* investigated the effects of varying the substrate density assuming that all the other parameters were constant. Density is not explicitly found in the model equations (2.1) - (2.2), but it is used in calculating some of the parameters of the model. The specific expressions for these parameters can be found in the original paper [Finger et al., 1976]. It was determined that at higher density values the rate of conversion was slightly higher, but the uniformity of conversion slightly decreased. Thus density was concluded not to be a major factor.

2.1.2 Summary and Discussion

The main ideas behind the model by Finger are as follows:

- The rate of biological degradation is proportional to the oxygen concentration in the gas phase of the compost matrix C^*.

- Arrhenius equation governs the dependence of the reaction rate on the temperature.

- The mechanism of oxygen supply is molecular diffusion.

- It is assumed that organic matter is abundant and therefore not a limiting factor for the reaction.

Finger's model, being a reaction-diffusion system, predicts steady-state profiles of temperature and oxygen. These distributions, as proposed by the authors, correspond to the thermophilic stage of composting when the conditions within the pile are relatively constant. Therefore, the model by Finger only considers one stage of composting and does not look at the process as a whole, from the beginning to the end of decomposition. This is due to the fact that Finger assumes abundance of organic matter and does not account for its depletion. The model also assumes that molecular diffusion is the primary way the oxygen is transfered into the pile from the outside environment. However, molecular diffusion is an extremely slow process. It has been shown that diffusion provides only a small percentage of oxygen needed in composting [Haug, 1993]. The primary mechanism of oxygen supply is the buoyant flow of air through the pile, or natural convection, which is not included in the model by Finger.

2.2 Models by Sidhu

The models by Sidhu were developed to study the phenomenon of self-ignition in compost piles. The models incorporate two terms for the heat release: biological heat and the heat of combustion. The first model by Sidhu predicts only the temperature profile, and the second model predicts oxygen concentration profile as well as the temperature profile. The geometry used for both models is a rectangular cross-section of a pile. The models are utilized to explore how the maximum temperature in the pile depends on its size, and what are the critical conditions for ignition. As self-ignition of compost piles is not the focus of this thesis, we will not describe the latter studies here.

2.2.1 Model I: Temperature Profile

The first model developed by Sidhu et al. [Sidhu et al., 2007b] predicts only the temperature profile of a compost windrow. Similarly to Finger's model, it reflects the steady-state profile of the temperature corresponding to the high-rate, or thermophilic, stage in composting. Sidhu's study focuses on the phenomenon of self-ignition, and thus includes chemical oxidation (combustion) heat in addition to the biological heat in the pile. In

this preliminary model, the oxygen is omitted, and the model consists of one equation for the temperature T:

$$(\rho C)_{eff}\frac{\partial T}{\partial t} = k_{eff}\Delta T + h_c(T) + h_b(T), \tag{2.9}$$

where

$$\begin{aligned} h_c(T) &= Q_c(1-\epsilon)\rho_c A_c \exp(-\frac{E_c}{RT}), & (2.10)\\ h_b(T) &= Q_b(1-\epsilon)\rho_b \frac{A_1 \exp(\frac{-E_1}{RT})}{1 + A_2 \exp(\frac{-E_2}{RT})}, & (2.11)\\ k_{eff} &= \epsilon k_{air} + (1-\epsilon)k_c, & (2.12)\\ (\rho C)_{eff} &= \epsilon \rho_{air} C_{air} + (1-\epsilon)\rho_c C_c. & (2.13) \end{aligned}$$

The parameters of the model are defined in Table 2.1. The first term on the right-hand side of equation (2.9) represents the diffusion of heat through the compost. Compared to Finger's model with one term describing the heat release, Sidhu's model contains two heat release terms: $h_b(T)$ and $h_c(T)$. $h_b(T)$ represents the heat released due to the biological activity in the pile. It is a bell-shaped function of the temperature T, reflecting the fact that at high temperatures biological activity in the pile ceases (see Figure 2.2.a). The term for the heat of combustion $h_c(T)$ is an Arrhenius-type term, and it increases exponentially with temperature (see Figure 2.2.b). The authors employ the model to study self-ignition in compost piles depending on their size, and also explore the effects of insulating the bottom of the piles.

2.2.2 Model II: Temperature and Oxygen Profiles

In 2007, Sidhu et al. extended the previous model to include oxygen [Sidhu et al., 2007a]. Throughout this thesis, we will refer to this extended model as the Sidhu II model. Similarly to the model described above, it focuses on studying self-ignition in compost piles and includes two terms for the heat release: a biological heat term $h_b(T)$ and a chemical, or combustion heat term $h_c(T)$. In this extended model, the chemical heat

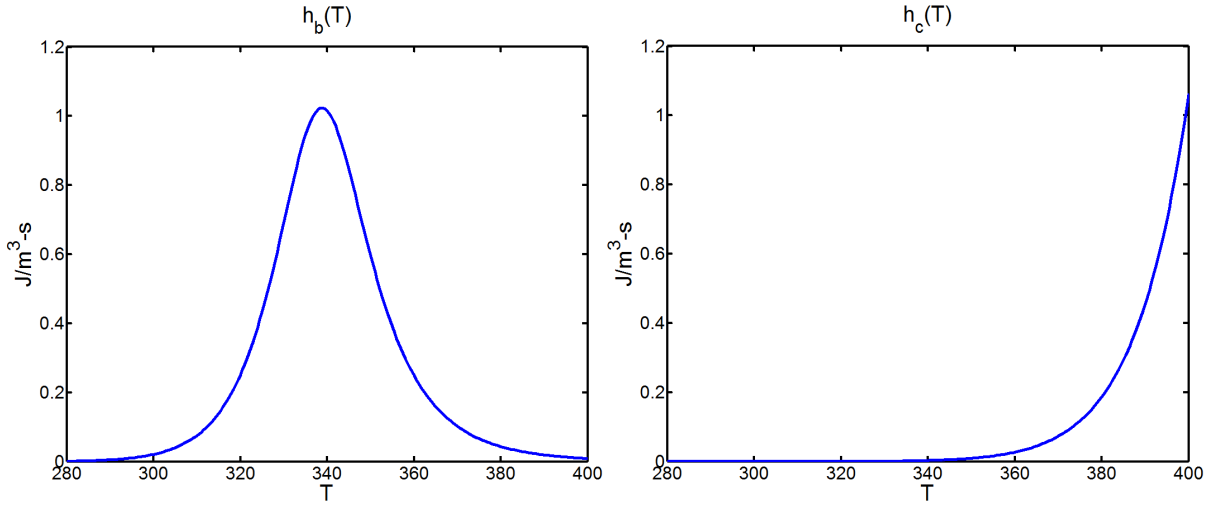

(a) (b)

Figure 2.2: Heat release terms plotted as a function of temperature T (K): (a) $h_b(T)$: heat released due to the biological activity in the pile as defined in equation (2.11), (b) $h_c(T)$: heat released due to the chemical oxidation, or combustion as defined in equation (2.10).

release is made proportional to the oxygen concentration, and the biological heat release is assumed not to be dependent on the oxygen. The model consists of two equations for temperature and oxygen concentration:

$$(\rho C)_{eff}\frac{\partial T}{\partial t} = k_{eff}\Delta T + h_c(T)O_2 + h_b(T), \tag{2.14}$$

$$\epsilon\frac{\partial O_2}{\partial t} = D_{o,eff}\Delta O_2 - A_c(1-\epsilon)\rho_c \exp\left(\frac{-E_c}{RT}\right)O_2, \tag{2.15}$$

where $h_c(T)$, $h_b(T)$, k_{eff}, and $(\rho C)_{eff}$ are defined by (2.10)-(2.13) and

$$D_{o,eff} = \epsilon D_{o,air}. \tag{2.16}$$

In the equation for temperature, (2.14), the first term on the right-hand side represents the diffusion of heat through the compost, the second term is the heat of combustion, and the third term is the biological heat. In the equation for oxygen concentration (2.15), the first term on the right-hand side represents molecular diffusion of oxygen through the pores of the composting material, and the second term, which is proportional to the oxygen concentration O_2, stands for the consumption of oxygen in the combustion

A_C	pre-exponential factor for the oxidation of the cellulosic material	$1.8 \times 10^4\ 1/s$
A_1	pre-exponential factor for the oxidation of the biomass growth	$2.0 \times 10^6\ 1/s$
A_2	pre-exponential factor for the inhibition of biomass growth	6.86×10^{30}
A_3	pre-exponential factor for the oxidation of the cellulosic material	$1.8 \times 10^4\ m^3/s\text{-}kg$
C_{air}	heat capacity of air	$1005\ J/(kg \cdot K)$
C_c	heat capacity of the cellulosic material	$3320\ J/(kg \cdot K)$
$D_{o,air}$	diffusion coefficient for oxygen	$1.0 \times 10^{-5} m^2/s$
$D_{o,eff}$	effective diffusion coefficient for oxygen	m^2/s
E_c	activation energy for the oxidation of the cellulosic material	$1.1 \times 10^5\ J/mol$
E_1	activation energy for the biomass growth	$1.0 \times 10^5 J \cdot mol/biomass$
E_2	activation energy for the inhibition of biomass growth	$2.0 \times 10^5\ J \cdot mol/biomass$
O_2	oxygen concentration within the pile	kg/m^3
Q_b	exothermicity for the oxidation of biomass per kg of dry cellulose	$6.66 \times 10^6 J/kg$
Q_c	exothermicity for the oxidation of the cellulosic material	$1.7 \times 10^7\ J/kg$
R	ideal gas constant	$8.314\ J/(K \cdot mol)$
T	temperature within the compost pile	K
k_{air}	effective thermal conductivity of air	$0.026\ W/(m \cdot K)$
k_c	effective thermal conductivity of cellulose	$0.3\ W/(m \cdot K)$
k_{eff}	effective thermal conductivity of the bed	$W/(m \cdot K)$
t	time	s
ϵ	void fraction	0.3
$(\rho C)_{eff}$	effective thermal capacity per unit volume of the bed	$J/(m^3 K)$
ρ_{air}	density of air	$1.17\ kg/m^3$
ρ_b	density of bulk biomass within the compost pile	$575\ kg/m^3$
ρ_c	density of pure cellulosic material	$1150\ kg/m^3$

Table 2.1: Parameters of the models by Sidhu and Luangwilai.

reaction. All the model parameters are presented in Table 2.1. We can see from equation (2.15) that the oxygen is assumed to be depleted in the combustion reaction only and not in the reaction of biological oxidation, which is a simplifying assumption. It should also be noted that equation (2.14) is dimensionally incorrect if oxygen concentration is measured in kg/m^3 as stated in the paper. In order for the units in this equation to be consistent, O_2 has to be dimensionless.

The model is utilized to study the maximum temperature in the pile depending on its size and to determine the critical conditions for self-ignition. We omit the description of these studies as the self-ignition phenomenon is not the focus of our work.

2.2.3 Summary and Discussion

The two models by Sidhu discussed above were developed to study self-ignition in compost piles. Therefore, they include two sources of heat: heat released due to combustion $h_c(T)$ and the biological heat term $h_b(T)$. The first model predicts only the temperature profile,

and the second model predicts oxygen profile as well as the temperature distribution. In the second model, the combustion heat release term is made proportional to the oxygen concentration, while the biological heat is assumed to be independent of the oxygen concentration. Therefore, oxygen is assumed to be consumed in the chemical oxidation reaction (combustion) only, and not in the biological oxidation reaction. This assumption is justified by the fact that the model was developed to study self-ignition in compost piles, and therefore the combustion reaction was of main interest. However, to study composting process for the purpose of better understanding and optimization, it is crucial to include the consumption of oxygen by the biological decomposition reaction, because it is known that low oxygen concentrations are common and can play an important role in the composting process.

Similarly to the model by Finger, Sidhu assumes that the mechanism by which the oxygen is transported into the pile is molecular diffusion. However, as noted before, the main driving force for the movement of oxygen is the buoyant flow of air and not the diffusion. The buoyant flow is not incorporated into the models by Sidhu. In addition, Sidhu's models, as the model by Finger, look at the steady-state temperature and oxygen profiles and neglect the consumption of the organic matter, and therefore allow the prediction of the temperature and oxygen distribution at the thermophilic stage of composting only.

2.3 Models by Luangwilai

The models by Luangwilai extend the latter model by Sidhu to include the effects of the air flow. The air flow removes the heat and carries the oxygen through the pile. The first model is one-dimensional, and it assumes the air flow to be constant throughout the domain. The second model considers a two-dimensional rectangular cross-section of a compost pile, and utilizes a prescribed air flow pattern. Similar to the models by Sidhu, the models by Luangwilai focus on the phenomenon of self-ignition. The models are used to determine the critical values of the pile size and air velocity that lead to ignition of compost. As the self-ignition of compost piles is not the focus of our work, we will not present the simulation results for these models here, but will rather briefly introduce the

model equations and look at how the air flow is incorporated.

2.3.1 Model I: One Spatial Dimension with Constant Air Flow

In the paper by Luangwilai et al. [2010], the second model by Sidhu is extended to include the air flow through the compost pile. We will later refer to this model as the Luangwilai I model. This preliminary model is one-dimensional. The equations of the model are as follows:

$$(\rho C)_{eff}\frac{\partial T}{\partial t} = k_{eff}\frac{\partial^2 T}{\partial x^2} - \epsilon\rho_{air}C_{air}U\frac{\partial T}{\partial x} + h_c(T)O_2 + h_b(T), \tag{2.17}$$

$$\epsilon\frac{\partial O_2}{\partial t} = D_{o,eff}\frac{\partial^2 O_2}{\partial x^2} - \epsilon U\frac{\partial O_2}{\partial x} - A_c(1-\epsilon)\rho_c \exp\left(\frac{-E_c}{RT}\right)O_2. \tag{2.18}$$

The velocity of air is assumed to be constant throughout the pile ($U,\ m/s$). The model has the same terms as the Sidhu II model, except for the second terms in both equations, which represent the cooling of the compost and the oxygen movement due to the air flow. All the parameters are defined in Table 2.1.

2.3.2 Model II: Two Spatial Dimensions with Prescribed Air Flow Pattern

Model I was later extended to two spatial dimensions by Luangwilai and Sidhu [2011]. We will later refer to this extended model as the Luangwilai II model. The authors consider a simplified rectangular geometry (Figure 2.3). In this model the air flow is not constant throughout the pile as in the previous model. Instead, in order to obtain the values for the air velocity components U_x and U_y, a stream function Ψ is introduced:

$$U_x = \frac{\partial \Psi}{\partial y}, \quad U_y = -\frac{\partial \Psi}{\partial x}, \tag{2.19}$$

where Ψ satisfies the equation

$$\frac{\partial^2 \Psi}{\partial x^2} + \frac{\partial^2 \Psi}{\partial y^2} = 0, \quad 0 \le x \le L \ , \ 0 \le y \le H. \tag{2.20}$$

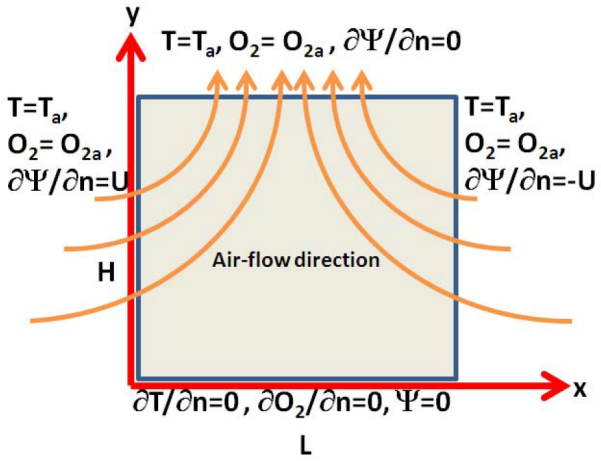

Figure 2.3: Diagram of a cross-section of a compost pile showing the direction of the air flow and the boundary conditions [Luangwilai and Sidhu, 2011].

The boundary conditions for Ψ are shown in Figure 2.3. The air is assumed to be entering the sides of the pile at a constant velocity U and coming out of the top of the pile in a strictly vertical direction. The equations of the model are similar to the Luangwilai I model, except in this extended model there are two spatial dimensions, and instead of the constant speed U there are two spatially varying velocity components U_x and U_y. The model equations are presented below:

$$\begin{aligned}(\rho C)_{eff}\frac{\partial T}{\partial t} &= k_{eff}\left(\frac{\partial^2 T}{\partial x^2}+\frac{\partial^2 T}{\partial y^2}\right)-\epsilon\rho_{air}C_{air}\left(U_x\frac{\partial T}{\partial x}+U_y\frac{\partial T}{\partial y}\right)\\ &\quad +h_c^*(T)O_2+h_b(T), \qquad (2.21)\\ \epsilon\frac{\partial O_2}{\partial t} &= D_{o,eff}\left(\frac{\partial^2 O_2}{\partial x^2}+\frac{\partial^2 O_2}{\partial y^2}\right)-\epsilon\left(U_x\frac{\partial O_2}{\partial x}+U_y\frac{\partial O_2}{\partial y}\right)\\ &\quad -A_3(1-\epsilon)\rho_c\exp\left(\frac{-E_c}{RT}\right)O_2, \qquad (2.22)\end{aligned}$$

where

$$h_c^*(T)=Q_c(1-\epsilon)\rho_c A_3\exp\left(-\frac{E_c}{RT}\right), \qquad (2.23)$$

and U_x and U_y are defined by equations (2.19) and (2.20). Expression for the heat release term $h_c(T)$ used in the models by Sidhu and in the Luangwilai I model and the expression for the heat release term $h_c^*(T)$ are similar (compare equations (2.10) and (2.23)), except in the expression for $h_c^*(T)$ parameter A_3 is used instead of A_C. This change corrects the dimensional inconsistency of the Sidhu II and Luangwilai I models (see the second term

on the right-hand side of equation (2.14) and the third term on the right-hand side of equation (2.17)).

2.3.3 Summary and Discussion

The Luangwilai I and II models incorporate the flow of air into the Sidhu II model. The air flow cools the substrate and carries the oxygen. The first model is one-dimensional and assumes the air flow speed to be constant throughout the composting material. In the second, two-dimensional model the air flow is not constant, however, the air flow pattern is still simplified. This model is only applicable for a rectangular cross-section of a compost pile. The air is assumed to be coming into the pile from both sides at a constant speed U and coming out of the top of the pile in a strictly vertical direction (see Figure 2.3). Therefore, the air flow pattern is prescribed and does not depend on the temperature within the pile. Similarly to the models by Finger and Sidhu, the models by Luangwilai neglect the consumption of organic matter and only model the temperature and oxygen distribution which corresponds to the thermophilic, or high-rate stage of composting.

3 Model Development

In Chapter 2, existing spatial models for composting were discussed. The properties of the existing spatial models for composting are summarized in Table 3.1:

Model properties:	Finger	Sidhu I	Sidhu II	Luangwilai I	Luangwilai II
Temperature	yes	yes	yes	yes	yes
Oxygen	yes	no	yes	yes	yes
Oxygen supply	diffusion	diffusion	diffusion	constant speed air flow	prescribed, constant air flow pattern
Geometry	any	any	any	1D	2D, a rectangle
Substrate consumption	no	no	no	no	no

Table 3.1: Existing model properties.

The existing models have the following shortcomings:

- neglect the consumption of organic matter and consider only the high-rate stage of composting when the organic matter is assumed to be abundant;
- assume that the mechanism of oxygen supply is molecular diffusion and do not account for the buoyant flow of air in the pile, or utilize a prescribed, constant air flow pattern;
- most models neglect the cooling of compost by air moving through the pile, and the models that do account for it (the Luangwilai I and II models) are only applicable for a simplified geometry (either one-dimensional or a two-dimensional rectangle).

In this chapter, we focus on the development of a new model for composting. The goal is to create a model that has the following features:

- accounts for the consumption of organic matter and therefore reflects the whole composting process, from the beginning to the end of decomposition;
- gives a realistic prediction of the air flow patterns within the compost pile;
- incorporates the cooling of the compost by passing air;

- is applicable for any one-, two-, or three-dimensional pile geometry;
- allows for inclusion of compaction effects.

The model has five dependent variables: temperature of the composting material T (K), temperature of the air inside the pores of the compost matrix T_{air} (K) (this variable allows us to account for the cooling of the compost by the air flow), oxygen concentration O_2 (kg/m^3_{air}), available substrate density S (kg/m^3), and pressure P (Pa). We will derive the equations of the model step by step. First, in Section 3.1, we will introduce the general form of the equations for temperature of the compost, oxygen concentration, and available substrate. Then, in Section 3.2, we will focus on choosing the specific expressions for biological decomposition reaction terms. In Section 3.3, we will add equations for the pressure P and for the temperature of the air T_{air}. In Section 3.4, we will present the complete set of equations and summarize the parameters of our model. Finally, in Section 3.5, we will introduce the effects of compaction and derive the expressions for the dependency of the air-filled porosity, permeability, and density on the depth.

3.1 Model Structure

In this section, we present the basic model structure and write the general form of the equations for the three main variables of our model: temperature of the composting material T, oxygen concentration O_2, and substrate density S. At this point, we will leave parts of the equations undefined, namely expressions for heat generated by bacteria, oxygen consumption, substrate consumption, and heat loss to the passing air. They will be determined in the following sections.

First, the equation for the *temperature* T takes a form similar to previous models:

$$\frac{\partial T}{\partial t} = D\Delta T + \text{heat generated} - \text{heat lost to the passing air.} \tag{3.1}$$

The first term on the right-hand side represents the dissipation of heat through the compost. Heat is generated in the biological decomposition reaction and lost to the air

passing through the composting material. The specific expressions for these terms will be chosen later.

The next variable of the model is the *oxygen concentration* O_2 (kg/m^3_{air}). We emphasize that the oxygen concentration is measured per cubic meter of air, because for the porous material the units m^3 and m^3_{air} are different and related by the following expression:

$$m^3_{air} = \Phi\ m^3, \tag{3.2}$$

where Φ is the air-filled porosity as described in Section 1.2.1. When defining the parameter units, we will always include the subscript "air" when referring to the volume of the air and not the volume of composting material. We use the generic transport and diffusion equation with a consumption term to describe the flow of air through the compost pile:

$$\frac{\partial O_2}{\partial t} + \vec{\nabla} \cdot (O_2 \vec{q}) = d\Delta O_2 - \text{consumption of oxygen}, \tag{3.3}$$

where d (m^2/hr) is the coefficient of molecular diffusion of oxygen in the air filling the porous space of the compost matrix. We assume that the volume flux of air $\vec{q}$ (m/hr) is known at each point within the pile. Oxygen will be carried by the air and, at the same time, molecular diffusion of oxygen in air will take place as well. The oxygen is also depleted in the biological oxidation reaction. The second term on the left-hand side of the equation is the convection term, representing that the oxygen is carried by the air, which has a volume flux $\vec{q}$ specified later, in Section 3.3. The first term on the right-hand side corresponds to the molecular diffusion of oxygen in air.

The last variable is the *substrate* S (kg/m^3), which will be simply consumed, and we add a small diffusion term to the equation for the substrate to ensure numerical stability of our model:

$$\frac{\partial S}{\partial t} = d_S \Delta S - \text{consumption of substrate}, \tag{3.4}$$

where d_S (m^2/hr) is a small diffusion coefficient. Adding the small diffusion term ensures smoothing of possible numerical errors.

It should be noted that the initial value of substrate density S will not be equal to the

bulk density of the composting material. The material will also contain water and other non-biodegradable components. Thus, in general, S is less than ρ, where ρ (kg/m^3) is the bulk density.

The next step in the development of the model is to complete the system of equations (3.1), (3.3), and (3.4) by choosing the expressions for the generated heat, heat lost to the passing air, oxygen and substrate consumption, and defining the volume flux of air $\vec{q}$, which is done in Sections 3.2 and 3.3.

3.2 Modeling the Reaction Rates

In this section, we will discuss how the biological oxidation reaction rates were modeled previously in the literature and present the expressions that we will use in our model. The rate of biological oxidation can be influenced by many factors such as temperature, oxygen availability, substrate availability, pH level, and moisture content. In our model, we will consider the most significant limitations caused by temperature, oxygen, and substrate availability only. Therefore, the heat release rate K_T (K/hr), the oxygen consumption rate K_{O_2} $(kg/hr\text{-}m^3_{air})$, and the rate of substrate consumption K_S $(kg/hr\text{-}m^3)$ will be considered as functions of the temperature, oxygen concentration, and available substrate:

$$K_T = K_T(T, O_2, S), \quad K_{O_2} = K_{O_2}(T, O_2, S), \quad K_S = K_S(T, O_2, S). \tag{3.5}$$

The rates of heat release, oxygen consumption, and substrate consumption are proportional to each other. They are connected by the stoichiometry of the biological oxidation reaction. Therefore, if one of the rates and the stoichiometric coefficients are known, all rates can be calculated. It is commonly assumed [Mason, 2008] that the effects of temperature, oxygen concentration, and substrate availability are multiplicative, so that

$$K_T = K_T^* f(T) g(O_2) h(S), \tag{3.6}$$

$$K_{O_2} = K_{O_2}^* f(T) g(O_2) h(S), \tag{3.7}$$

$$K_S = K_S^* f(T) g(O_2) h(S), \tag{3.8}$$

where $f(T)$, $g(O_2)$, and $h(S)$ are the correction factors for temperature, oxygen concentration, and substrate availability, respectively. Below we discuss the expressions used for these factors.

3.2.1 Temperature Correction Factor

The effect of temperature on the rate of biological oxidation has been incorporated in many models for composting, both spatial and non-spatial. In the model by Finger, the heat release term has the following form:

$$K_T = K_T^* \exp\left(\frac{-E_a}{RT}\right) O_2 = K_T^* f(T) g(O_2), \tag{3.9}$$

where $f(T) = \exp(\frac{-E_a}{RT})$ and $g(O_2) = O_2$. As discussed in Section 2.1, Finger uses the Arrhenius equation to describe how temperature affects the reaction rate. He also assumes the heat release rate to be proportional to the oxygen concentration O_2. It should be noted that in Finger's model, the temperature correction factor is unbounded, and the reaction rate can be very large at high temperatures. However, oxygen concentration serves as a limiting factor. Sidhu used the following correction term for the temperature:

$$f(T) = Q_b(1-\epsilon)\rho_b \frac{A_1 \exp\left(\frac{-E_1}{RT}\right)}{1 + A_2 \exp\left(\frac{-E_2}{RT}\right)}. \tag{3.10}$$

This is a bell-shaped curve with a maximum value of 1 at approximately 340 K (see Figure 2.2(a)). It reflects the fact that at very high temperatures biological activity in the pile ceases. Haug [1993] used the following expression to describe the temperature effect (see Figure 3.1):

$$f(T) = k_{20}(1.066^{(T-20)} - 1.21^{(T-60)}). \tag{3.11}$$

Liang et al. [2004] used the following piecewise function (see Figure 3.2):

$$f(T) = \begin{cases} 0.033 * T, & 0 \leq T \leq 30 \\ 1, & 30 \leq T \leq 55 \\ -0.05T + 3.75, & 55 \leq T \leq 75 \\ 0, & T \geq 75 \end{cases} \tag{3.12}$$

We choose to use the function $f(T)$ defined in (3.12) by Liang because of its simplicity and a good agreement between Liang's model predictions and the experimental data.

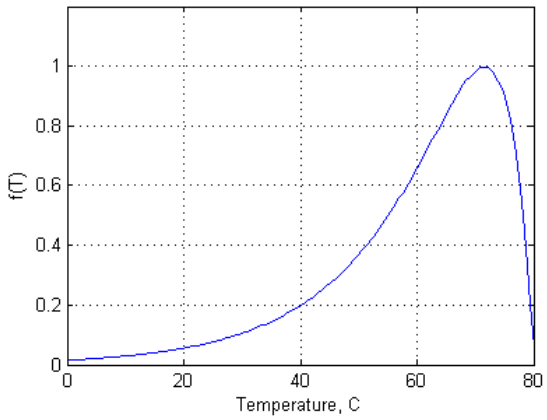

Figure 3.1: Temperature correction factor $f(T)$ as defined in equation (3.11), used by Haug [1993].

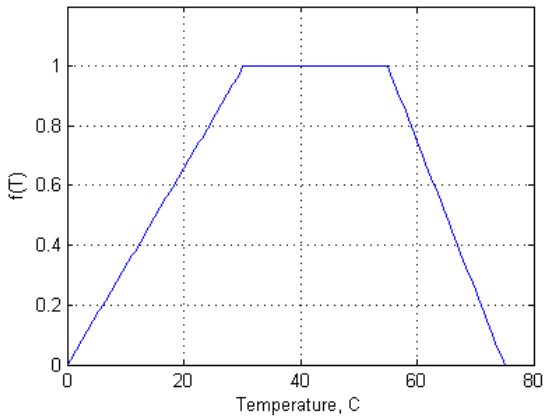

Figure 3.2: Temperature correction factor $f(T)$ as defined in equation (3.12), used by Liang et al. [2004].

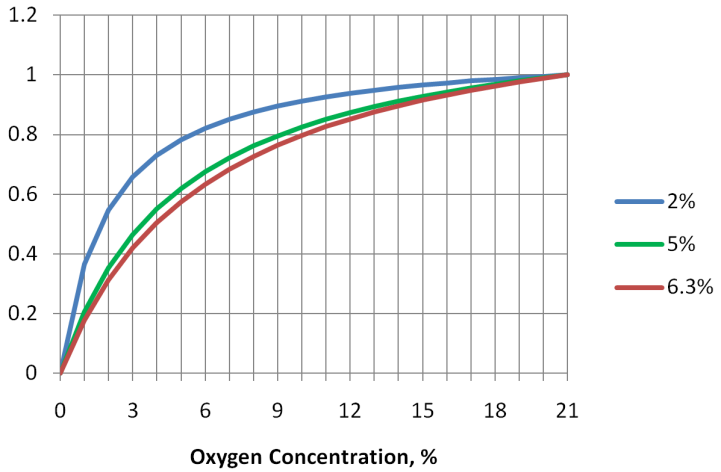

Figure 3.3: Oxygen correction factor $g(O_2)$ as defined in equation (3.14) for different values of the half-saturation constant H_{O_2}.

3.2.2 Oxygen Concentration Correction Factor

The oxygen concentration correction factor commonly is monod-type:

$$g(O_2) = \frac{O_2}{H_{O_2} + O_2}, \tag{3.13}$$

where H_{O_2} is the half-saturation constant. In our model, we will normalize the expression in (3.13) so that it takes the value of 1 when the oxygen concentration is equal to the ambient concentration O_2^{amb}:

$$g(O_2) = \frac{O_2}{H_{O_2} + O_2} \frac{H_{O_2} + O_2^{amb}}{O_2^{amb}}, \quad g(O_2^{amb}) = 1. \tag{3.14}$$

This expression was referred to by Richard et al. [2006] as the modified one-parameter model. The half-saturation constant H_{O_2} has been reported to have a range of values in the literature. Haug [1993, p. 401] assumed the half-saturation constant value to be 2% by volume. Stombaugh and Nokes [1996] assumed an H_{O_2} equal to 6.3%. We assume H_{O_2} to be equal 5%. This value becomes 0.2784 kg/m^3_{air} when converted to the units used in our model. Figure 3.3 shows the oxygen correction factor graphs for three different values of the half-saturation constant H_{O_2}.

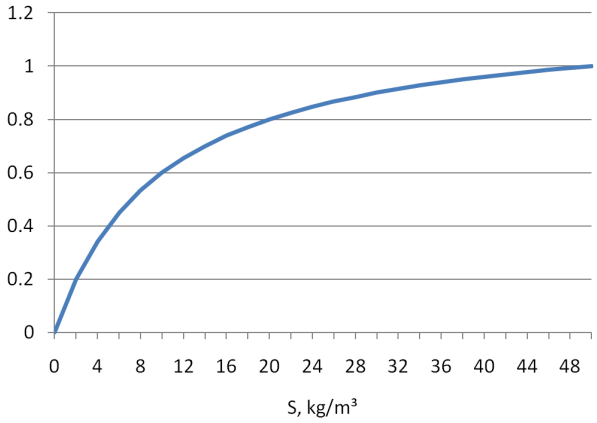

Figure 3.4: Substrate correction factor $h(S)$ as defined in equation (3.15) ($S_0 = 50\ kg/m^3$).

3.2.3 Substrate Correction Factor

For the substrate correction factor, we use the following normalized monod-type expression (see Figure 3.4):

$$h(S) = \frac{6}{5}\frac{S}{S + S_0/5}, \quad h(S_0) = 1, \tag{3.15}$$

where S_0 (kg/m^3) is the initial substrate density. We assume the half-saturation constant to be equal to $S_0/5$. This reflects the idea that the substrate availability will not be a limiting factor until there is only a small amount of available substrate left.

3.3 Modeling the Air Flow.

So far, the model consists of equations (3.1), (3.3) and (3.4). In order to complete the model, it is required to determine the volume flux $\vec{q}$. To describe the flow of air through compost, we employ Darcy's Law with buoyancy derived in Section 1.2.2, namely equation (1.13), which we restate here:

$$\vec{q} = -\frac{k}{\mu}(\nabla P - C_{air}^{amb}\Phi g(1 - \frac{T_{amb}}{T_{air}})\vec{e_z}). \tag{3.16}$$

It can be observed from equation (3.16) that when the temperature T_{air} is equal to the ambient temperature T_{amb}, the buoyancy term vanishes. When $T_{air} > T_{amb}$, the air will move up in the direction $\vec{e_z}$. Darcy's Law introduces a new independent variable, namely

pressure P, and therefore one more equation is required to complete the model.

When studying natural convection, the Boussinesq approximation is commonly used [Nield and Bejan, 2006]. It allows us to assume that the flow is incompressible, except in the term accounting for buoyancy (second term in equation (3.16)). Applying the Boussinesq approximation, we complete our system with the equation of continuity for an incompressible flow:

$$\nabla \cdot \vec{q} = 0. \tag{3.17}$$

The equations we have developed so far are summarized below:

$$\begin{aligned}
\frac{\partial T}{\partial t} &= D\Delta T + K_T^* f(T)g(O_2)h(S) - \text{heat loss to passing air}, && (3.18)\\
\frac{\partial O_2}{\partial t} + \vec{\nabla} \cdot (O_2 \vec{q}) &= d\Delta O_2 - K_{O_2}^* f(T)g(O_2)h(S), && (3.19)\\
\frac{\partial S}{\partial t} &= d_S \Delta S - K_S^* f(T)g(O_2)h(S), && (3.20)\\
\vec{q} &= -\frac{k}{\mu}(\nabla P - C_{air}^{amb}\Phi g(1 - \frac{T_{amb}}{T})\vec{e_z}), && (3.21)\\
\nabla \cdot \vec{q} &= 0, && (3.22)
\end{aligned}$$

where $f(T)$, $g(O_2)$, and $h(S)$ are as given in (3.12), (3.14), and (3.15), respectively.

We now make a final step in our model development and incorporate *heat loss to passing air*. This is crucial because if cooling is not incorporated, more air flow only implies that more oxygen is supplied to the system and thus always serves as a positive factor. However, in reality, air flow cools the compost, and if the flow is very strong this cooling may be undesirable. To incorporate the cooling by the flowing air, we now include an additional dependent variable T_{air} (K), which represents the temperature of the air inside the pores of the composting material. As the cool air enters the pile, it heats from the compost matrix. A reverse process may also take place: if the air warms up in one part of the pile and then enters a cooler part, it may loose its heat to the cooler composting material. The air will move through the pile and exchange its thermal energy

with the composting matrix. The equation for the air temperature has the following form:

$$\frac{\partial T_{air}}{\partial t} + \vec{\nabla} \cdot (T_{air}\vec{q}) = d_{air}\Delta T_{air} + \text{heat received from the compost matrix}, \tag{3.23}$$

where d_{air} (m^2/hr) is the thermal diffusivity of air in the pores of composting material. The second term on the left side of the equation is a convection term reflecting the movement of air. The first term on the right side is a diffusion term, which represents the diffusion of heat through the air.

In order to mathematically describe the heat exchange between the compost matrix and the air, we assume this exchange occurs through the surface area of the porous compost matrix. To describe that area, we introduce a new parameter a (m^2_{area}/m^3), which characterizes the size of the area available for the heat exchange. For simplicity, we assume that the Newton's law of cooling holds and that the rate of heat exchange is proportional to the temperature difference. Therefore, the equations for the temperature T (3.18) and air temperature T_{air} (3.23) can be completed in the following way:

$$\begin{aligned}
\frac{\partial T}{\partial t} &= D\Delta T + K_T^* f(T)g(O_2)h(S) - \beta(T - T_{air}), && (3.24)\\
\frac{\partial T_{air}}{\partial t} + \vec{\nabla} \cdot (T_{air}\vec{q}) &= d_{air}\Delta T_{air} + \alpha(T - T_{air}), && (3.25)\\
\alpha &= \frac{aU}{\Phi\lambda_{air}C_{air}^{amb}}, && (3.26)\\
\beta &= \frac{aU}{\lambda\rho}, && (3.27)
\end{aligned}$$

where α and β are coefficients that characterize the speed of the temperature change of air and composting material, respectively. Parameter α is calculated using the surface area per unit volume a, the overall heat transfer coefficient U, the heat capacity of air λ_{air}, and the air density C_{air}^{amb}. To calculate β, we use the heat capacity of the composting material λ and the bulk density ρ. All the parameters used to compute α and β can be found in Table 3.2.

3.4 Complete Model Formulation

Combining all our derivations, we present the complete model:

$$\frac{\partial T}{\partial t} = D\Delta T + K_T^* f(T)g(O_2)h(S) - \beta(T - T_{air}), \tag{3.28}$$

$$\frac{\partial T_{air}}{\partial t} + \vec{\nabla} \cdot (T_{air}\vec{q}) = d_{air}\Delta T_{air} + \alpha(T - T_{air}), \tag{3.29}$$

$$\frac{\partial O_2}{\partial t} + \vec{\nabla} \cdot (O_2\vec{q}) = d\Delta O_2 - K_{O_2}^* f(T)g(O_2)h(S), \tag{3.30}$$

$$\frac{\partial S}{\partial t} = d_S\Delta S - K_S^* f(T)g(O_2)h(S), \tag{3.31}$$

$$\vec{q} = -\frac{k}{\mu}(\nabla P - C_{air}^{amb}\Phi g(1 - \frac{T_{amb}}{T_{air}})\vec{e_z}), \tag{3.32}$$

$$\nabla \cdot \vec{q} = 0, \tag{3.33}$$

where $f(T)$ is defined by (3.12), $g(O_2)$ by (3.14), $h(S)$ by (3.15), and α and β by (3.26) and (3.27). All the model parameters are summarized in Table 3.2. The developed model accounts for the buoyant flow of air through the pile and predicts the air flow patterns, includes cooling of the composting material by the air passing through it, and incorporates the consumption of substrate, therefore looking at the process from the beginning to the end of decomposition.

Compaction effects can be included into the model by considering some of the model parameters to be functions of depth. In the next section, we will incorporate compaction into our model by deriving the expressions for air-filled porosity, permeability, and density. In Chapter 4, we will use these expressions to calculate a number of other model parameters, therefore making them depth-dependent as well.

a	interfacial area	m^2/m^3
C_{air}^{amb}	ambient air density	kg/m^3_{air}
D	thermal diffusivity of the composting material	m^2/hr
d	diffusion coefficient for oxygen in the air filling the porous space	m^2/hr
d_{air}	thermal diffusivity of air	m^2/hr
d_S	substrate diffusion coefficient added for stability	m^2/hr
g	gravitational acceleration	$9.8\ m/s^2$
H_{O_2}	oxygen half-saturation constant	kg/m^3_{air}
k	permeability	m^2
$K^*_{O_2}$	maximum rate of oxygen consumption	kg/m^3_{air}-hr
K^*_T	maximum rate of heating	K/hr
K^*_S	maximum rate of substrate consumption	kg/m^3-hr
O_2	oxygen concentration in the air filling the pores of the compost matrix	kg/m^3_{air}
O_2^{amb}	ambient oxygen concentration	kg/m^3_{air}
P	pressure	Pa
S	available substrate density	kg/m^3
S_0	initial substrate density	kg/m^3
t	time	hr
T	temperature of the composting material	K
T_{air}	temperature of the air inside the pores of the compost matrix	K
T_{amb}	ambient temperature	K
U	overall heat transfer coefficient	J/K-hr-m^2
α	coefficient characterizing the rate of heating of the air from the compost	$1/hr$
β	coefficient characterizing the rate of cooling of the compost to the air	$1/hr$
Φ	air-filled porosity	1
ρ	bulk density of the composting material	kg/m^3
λ	heat capacity of the composting material	J/kg-K
λ_{air}	heat capacity of air	J/kg-K
μ	viscosity of air	$Pa \cdot hr$

Table 3.2: Parameter list for the complete model formulation, equations (3.28) - (3.33).

3.5 Compaction effects

In this section, we will derive expressions for depth-dependency of air-filled porosity, permeability, and density, which will be used later in Chapter 4 to include the effects of compaction into the model. A number of other model parameters will be calculated as functions of air-filled porosity and density, and therefore will depend on the depth as well.

The expressions for air-filled porosity, permeability, and density will be derived using the following expression for the compaction factor $h_i(d)$ presented by Das and Keener [1997]:

$$h_i(d) = h_\infty + \Delta h_0 \cdot \exp(-\delta \sigma_i(d)), \tag{3.34}$$

$$\sigma_i(d) = \rho_0 g d / 1000, \tag{3.35}$$

where $\sigma_i(d)$ (Pa) is the compressive stress at depth d (m), ρ_0 (kg/m^3) is the initial bulk density of the compost, and g (m/s^2) is the gravitational acceleration. The compaction factor $h_i(d)$ is a number between 0 and 1 which expresses the ratio between the thickness of the compacted layer of compost and the initial thickness of that layer, h_∞ represents the maximum compressed state when the stress σ_i is very large, Δh_0 is the total compressible fraction, $h_\infty + \Delta h_0 = 1$, and δ $(1/Pa)$ is the rate of volume reduction. In the following sections, we will derive the expressions for air-filled porosity, permeability, and density as functions of depth d using the compaction factor $h_i(d)$.

3.5.1 Effects of Compaction: Porosity

We now derive an expression to calculate the air-filled porosity value of the compacted material depending on the depth. Let V^1 be the volume of a layer of compost before the compaction. The volume consists of solids and water V^1_{sol+w} and air V^1_{air}:

$$V^1 = V^1_{sol+w} + V^1_{air}. \tag{3.36}$$

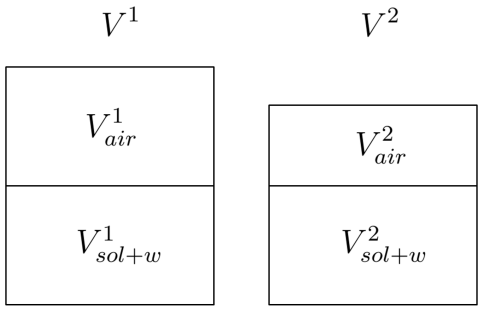

Figure 3.5: Compaction diagram.

After applying the stress $\sigma_i(d)$, the volume V^1 will be compacted to volume $V^2(d)$. The solids and water are assumed incompressible (see Figure 3.5). The ratio between the compacted volume $V_2(d)$ and initial volume V_1 is equal to the compaction factor $h_i(d)$:

$$h_i(d) = \frac{V^2(d)}{V^1}. \tag{3.37}$$

The volume $V^2(d)$ will contain the same volume of solids and water $V^2_{sol+w} = V^1_{sol+w}$, and a smaller volume of air $V^2_{air}(d)$:

$$V^2(d) = V^2_{sol+w} + V^2_{air}(d). \tag{3.38}$$

Subtracting equation (3.38) from (3.36), we obtain the following expression:

$$V^1 - V^2(d) = V^1_{air} - V^2_{air}(d). \tag{3.39}$$

Dividing equation (3.39) by V^1 and applying equation (3.37), we get the expression

$$1 - \frac{V^2(d)}{V^1} = \frac{V^1_{air}}{V^1} - \frac{V^2_{air}(d)}{V^1} = \frac{V^1_{air}}{V^1} - \frac{V^2(d)}{V^1}\frac{V^2_{air}(d)}{V^2(d)}, \text{ or } 1 - h_i(d) = \Phi^1 - h_i(d)\Phi^2(d), \tag{3.40}$$

where $\Phi^1 = V^1_{air}/V^1$ is the initial air-filled porosity and $\Phi^2(d) = V^2_{air}(d)/V^2(d)$ is the air-filled porosity after compaction. Using equation (3.40), we can now write the air-filled porosity after compaction as a function of the compaction factor $h_i(d)$ and the initial air-filled porosity Φ^1:

$$\Phi^2(d) = \frac{1}{h_i(d)}(\Phi^1 - 1) + 1. \tag{3.41}$$

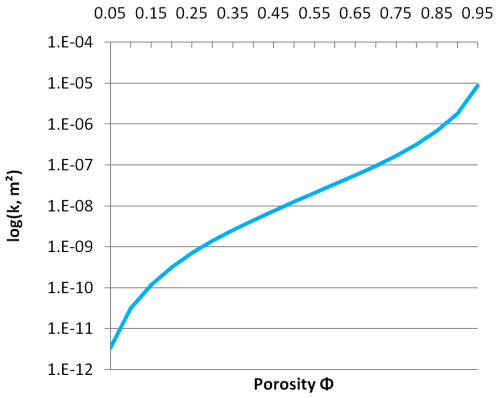

Figure 3.6: The dependence of the permeability on air-filled porosity according to the Kozeny-Carman model ($C = 4e7\ 1/m^2$), as defined by equation (3.42).

3.5.2 Effects of Compaction: Permeability

To estimate the permeability of the composting material, we apply the Kozeny-Carman model [Das and Keener, 1997]. This model relates the value of permeability k to the value of air-filled porosity Φ:

$$k(d) = \frac{\Phi(d)^3}{C(1 - \Phi(d))^2}, \tag{3.42}$$

where C $(1/m^2)$ is the Kozeny-Carman constant. Porosity, and therefore the permeability, depend on the depth d. The Kozeny-Carman constant depends on the structure of the compost matrix and can take a wide range of values for different materials. In Chapter 4, we will determine the value of this constant by fitting our model to the experimental data. The graph of this function is presented in Figure 3.6 with the Kozeny-Carman constant value of $4e7\ 1/m^2$.

3.5.3 Effects of Compaction: Density

To derive an expression for density variation with depth, we will use the same notation as in our derivation of the expression for air-filled porosity in Section 3.5.1. Recall that V^1 is the volume of a layer of compost before compaction, and V^2 is the volume of that layer after compaction. The mass of the compost m (kg) will stay the same. Therefore, we can obtain an expression for the density after compaction $\rho_2(d)$:

$$\rho_2(d) = \frac{m}{V^2} = \frac{m}{V^1}\frac{V^1}{V^2} = \frac{\rho_1}{h_i(d)}. \tag{3.43}$$

4 Model Validation

To validate our model, we use the experimental data provided to us by S. Yu [Yu, 2007]. Yu explored the effects of varying the free air space on composting kinetics. A series of experiments was conducted in which composting was carried out in laboratory conditions in a cylindrical vessel as shown in Figure 4.1. For each of the four experiments, or treatments, a different value of air-filled porosity was achieved by adding wood chips to the composting material. During the course of every experiment, the temperature values were recorded at different locations in the vessel (see Figure 4.1), and the air flow rates were measured at the inlet and at the outlet of the vessel.

In Section 4.1, we describe the four experiments conducted in more detail. In Section 4.2, we explain how our model can be applied to simulate these experiments and present the values for the model parameters used in the simulations. We fix the parameters which have well-established values and vary the parameters that have a range of reported values in the literature to find a set that yields good agreement between the model's predictions and the experimental temperature and air flow data. The complete set of parameters was first determined by fitting the model to the data for Treatment 3. The predictions for other treatments were obtained by varying a small number of parameters from this set to reflect the changes in substrate composition for each treatment. All the parameters that have the same values for all the four treatments are listed in Table 4.2 . The parameters that varied from one treatment to another are presented in Table 4.3. The parameter values determined in this chapter will be utilized for windrow simulations in Chapter 5.

4.1 Review of the Experimental Setup

The four treatments were carried out in laboratory conditions in a cylindrical vessel shown in Figure 4.1. The vessel had a diameter of 0.6 meters and a height of 0.9 meters. The vessel had an open mesh bottom to allow air to enter freely and the sides of the vessel were insulated. The composting material consisted of dairy manure, wood chips, sawdust, and canola straw. The initial moisture content of the mixture was 76%. The

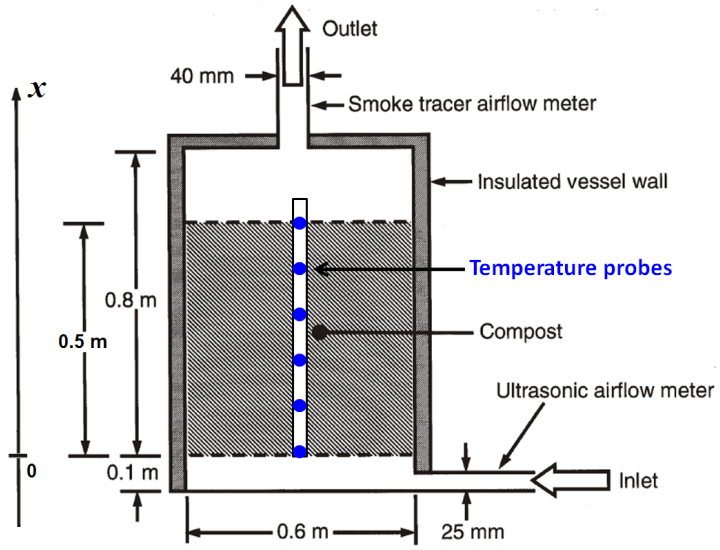

Figure 4.1: Composting vessel diagram. Modified from Yu et al. [2005].

	Treatment 1	Treatment 2	Treatment 3	Treatment 4
Φ_0	44.5%	52.1%	57.1%	64.5%
$\rho_0(kg/m^3)$	630.0	558.1	520.1	466.2

Table 4.1: Values of the initial air-filled porosity Φ_0 and bulk density ρ_0 for the four experimental treatments in Yu [2007].

average ambient temperature in the lab was $23.3°C$ and the average relative humidity was 56.4%. At the beginning of each of the experiments, the vessel was filled to a height of 0.5 meters.

The experiments were conducted for four different air-filled porosity values which where achieved by adding different amounts of wood chips to the mixture. In each treatment, temperature was recorded at six points along the midline of the vessel. The points were vertically separated by 0.1 meters (see Figure 4.1). The initial air-filled porosity and density values for the four mixtures were measured and are presented in Table 4.1. The data obtained along with our model's predictions will be presented later in Section 4.3.

4.2 Model Setup

In this section, we describe how we apply our model to the experimental setup described above. We discuss the domain of the model, and the boundary and initial conditions

used for each of the independent variables of the model.

The sides of the vessel are insulated and therefore we can assume that all the variables of interest change only from the bottom to the top of the vessel, and we can neglect the variation in the horizontal plane. This assumption was confirmed experimentally when the temperature was measured away from the center line of the vessel. It was found that the temperature difference between the measured values and the center line values was small and never exceeded $3°C$. Assuming that the variables of the model vary only from the bottom to the top of the vessel, we can use the interval [0, 0.5 m] as a simple one-dimensional domain for our model equations. Using a one-dimensional domain significantly decreases the computation time and allows for more efficient fitting of the parameter values to data. We use one spatial variable x which represents the distance in meters measured from the bottom of the vessel (see Figure 4.1). The initial conditions we choose are as follows:

$$\begin{aligned} T(0,x) =& T_{amb}, \quad T_{air}(0,x) = T_{amb}, \quad O_2(0,x) = O_2^{amb}, \\ & S(0,x) = S_0, \quad P(0,x) = P_{atm}, \end{aligned} \tag{4.1}$$

where $T_{amb} = 23.3°C$ is the average ambient temperature, $O_2^{amb} = 0.2784\ kg/m^3_{air}$ is the ambient oxygen concentration, S_0 is the initial available substrate density, and $P_{atm} = 101325\ Pa$ is the standard atmospheric pressure. The value for the initial substrate availability S_0 varies for the four experiments conducted, because in each experiment the composting material had a different amount of wood chips, which are considered inert, and therefore the amount of organic mater available for the biological decomposition changed from one experiment to another. The formula by which S_0 is calculated is presented in Table 4.3.

We use Dirichlet boundary conditions for the temperature of the air T_{air}, pressure P,

and oxygen concentration O_2 on both ends of the domain:

$$T_{air}(t,0) = T_{air}(t,0.5) = T_{amb}, \tag{4.2}$$

$$P(t,0) = P(t,0.5) = P_{atm}, \tag{4.3}$$

$$O_2(t,0) = O_2(t,0.5) = O_2^{amb}. \tag{4.4}$$

The substrate does not leave or enter the vessel and therefore on both ends of the domain we apply the no-flux condition for the available substrate S:

$$\frac{\partial S}{\partial \vec{n}}(t,0) = \frac{\partial S}{\partial \vec{n}}(t,0.5) = 0, \tag{4.5}$$

where $\vec{n}$ is an outward normal unit vector. For the temperature T of the composting material, we use a flux condition determined by Newton's law of cooling:

$$\frac{\partial T}{\partial \vec{n}}(t,0) = \frac{\partial T}{\partial \vec{n}}(t,0.5) = -\frac{U}{\lambda \rho D}(T - T_{amb}), \tag{4.6}$$

where U is the overall heat transfer coefficient, λ is the heat capacity of the composting material, ρ is the bulk density of the material, and D is the thermal diffusivity. This sets the heat flux through the boundary to be proportional to the temperature difference between the compost and the outside environment. This boundary condition has not been used in any of the existing spatial models for composting discussed in Chapter 2. Instead, the temperature of the compost on the edges of the domain was usually assumed to be equal to the ambient temperature, or the no-flux condition was applied for insulated boundaries. However, the experimental data clearly shows that the temperature of the compost on the edges is significantly higher than the ambient temperature, and therefore the flux boundary condition has been adopted.

Our model equations (3.28) - (3.33) take the following form in one dimension:

$$\frac{\partial T}{\partial t} = D\frac{\partial^2 T}{\partial x^2} + K_T^* f(T)g(O_2)h(S) - \beta(T - T_{air}), \tag{4.7}$$

$$\frac{\partial T_{air}}{\partial t} + \frac{\partial}{\partial x}(T_{air}q) = d_{air}\frac{\partial^2 T_{air}}{\partial x^2} + \alpha(T - T_{air}), \tag{4.8}$$

$$\frac{\partial O_2}{\partial t} + \frac{\partial}{\partial x}(O_2 q) = d\frac{\partial^2 O_2}{\partial x^2} - K_{O_2}^* f(T)g(O_2)h(S), \tag{4.9}$$

$$\frac{\partial S}{\partial t} = d_S\frac{\partial^2 S}{\partial x^2} - K_S^* f(T)g(O_2)h(S), \tag{4.10}$$

$$q = -\frac{k}{\mu}(\frac{\partial P}{\partial x} - C_{air}^{amb}\Phi g(1 - \frac{T_{amb}}{T_{air}})), \tag{4.11}$$

$$\frac{\partial q}{\partial x} = 0. \tag{4.12}$$

We can see that for the one-dimensional case, the incompressibility condition (4.12) simply means that the volume flux of air q is constant throughout the domain.

We incorporate the effects of compaction into our simulations using the equations that were discussed in Section 3.5 with parameter values taken from Das and Keener [1997]:

$$h_i(x) = 0.604 + 0.396\exp(-0.105\rho_0(0.5 - x)g/1000), \tag{4.13}$$

$$\Phi(x) = \frac{1}{h_i(x)}(\Phi_0 - 1) + 1, \tag{4.14}$$

$$k(x) = \frac{\Phi(x)}{C(1 - \Phi(x))^2}, \tag{4.15}$$

$$\rho(x) = \frac{\rho_0}{h_i(x)}, \tag{4.16}$$

where all the parameter values are listed in Table 4.3. For simplicity, we use the same parameters in equation (4.13) for the compaction of the composting materials in all four cases, even though the composition of the substrate varies and in reality the parameters may vary. The variation of air-filled porosity and density with depth according to equations (4.14) and (4.16) is shown in Figure 4.2 for all four treatments.

In equation (4.15), the permeability k is determined by air-filled porosity Φ and the Kozeny-Carman constant C. This constant, as described in Section 3.5.2, depends on the structure of the compost matrix and therefore may vary from one experiment to another. We determined the value of C for each of the experiments by fitting the model to the

experimental data focusing mainly on the air flow data (see Section 4.3.5).

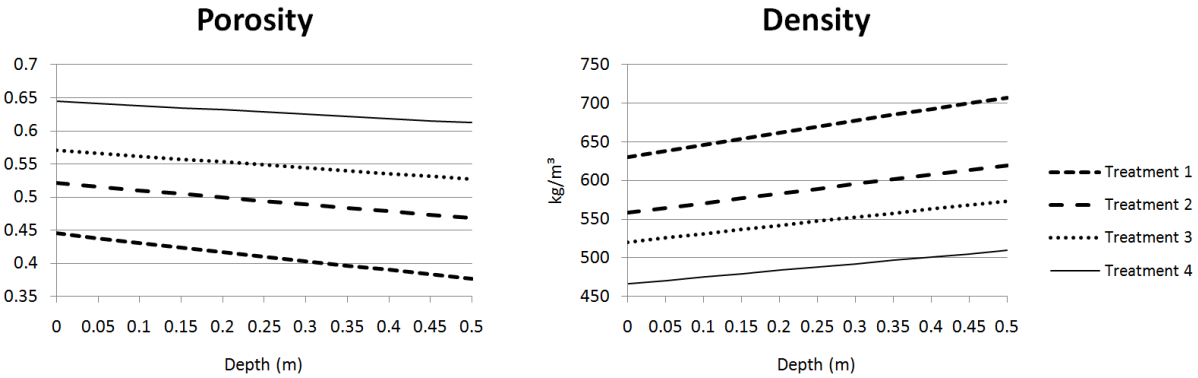

Figure 4.2: Air-filled porosity and density variations with depth for the four treatments as defined in equations (4.14) and (4.16).

Parameter	Value	Comments
C_{air}^{amb} (kg/m_{air}^3)	1.2	We used the value for the ambient air density at $20°C$ and standard atmospheric pressure $P_{atm} = 101325\ Pa$.
d (m^2/hr)	$0.0576 \cdot 0.5$	The coefficient of molecular diffusion of oxygen was estimated as half of the diffusion coefficient for carbon dioxide in air. Division by 2 was done to approximately account for the fact that only the porous space of the compost matrix is available for oxygen diffusion.
d_{air} (m^2/hr)	$0.0684 \cdot 0.5$	Thermal diffusivity of air was divided by 2 to account for the fact that the air is located in the pores of the compost matrix.
d_S (m^2/hr)	1e-6	A small substrate diffusion coefficient was added to improve numerical stability of the model.
g (m/s^2)	9.8	Gravitational acceleration.
H_{O_2} (kg/m_{air}^3)	6.63e-2	As discussed in Section 3.2.2, the half-saturation constant for oxygen was assumed to be 5% by volume (ambient oxygen content is 21% by volume). This value was then converted into kg/m_{air}^3.
K_S^* $(kg/m^3\text{-}hr)$	0.45	The value of the maximum substrate consumption rate was obtained by fitting the model to the experimental data from Yu [2007].
$K_{O_2}^*(x)$ $(kg/m_{air}^3\text{-}hr)$	$\frac{Y_{O/S}K_S}{\Phi(x)}$	The maximum oxygen consumption rate is calculated using the stoichiometric coefficient $Y_{O/S}$ and the air-filled porosity value $\Phi(x)$. Note that the air-filled porosity varies with depth. Therefore, the maximum oxygen consumption rate is a function of depth.
$K_T^*(x)$ (K/hr)	$\gamma\frac{Y_{H/S}K_S}{\lambda\rho(x)}$	The maximum rate of heat release is calculated using the stoichiometric coefficient $Y_{H/S}$, heat capacity of the compost λ, and bulk density ρ. It is then multiplied by a fraction γ which represents the percentage of energy derived from the decomposition of organic matter that will be used for heating the compost. The value of γ was obtained by fitting the model to the data from Yu [2007].
O_2^{amb} (kg/m_{air}^3)	$0.232 \cdot C_{air}^{amb}$	The ambient oxygen concentration was calculated as 23.2% by mass of the ambient air density [Haug, 1993].
P_{atm} (Pa)	101325	Standard atmospheric pressure.

Parameter	Value	Comments
T_0 (K)	273.15	Parameter used for converting the temperature value from $°C$ to K. The freezing point of water is $0°C$, or $273.15K$.
T_{amb} (K)	$23.3 + T_0$	Ambient temperature.
U $(\frac{J}{K\text{-}hr\text{-}m^2})$	700	The overall heat transfer coefficient was modified from Liang et al. [2004], where it was reported as 1000 $\frac{J}{K\text{-}hr\text{-}m^2}$. We used a smaller value because our model already accounts for the heat lost to the passing air.
$Y_{H/S}$ (J/kg)	1.91e7	The stoichiometric coefficient $Y_{H/S}$ determines how much energy is released from oxidation of a kg of substrate. The value was taken from Liang et al. [2004].
$Y_{O/S}$ (kg/kg)	1.37	The stoichiometric coefficient $Y_{O/S}$ determines how much oxygen is needed to oxidize a kg of substrate. The value was taken from Liang et al. [2004].
α $(1/hr)$	4933	α characterizes the temperature change of air and it was calculated using equation (3.26) with the value for initial air-filled porosity for Treatment 1. It was then kept constant for all other treatments for simplicity. The value of parameter a was estimated to be 2700 $1/m$ by fitting the model to the experimental data from Yu [2007].
β $(1/hr)$	1.19	β characterizes the temperature change of the composting material, it was calculated using equation (3.27) with the value of initial bulk density for Treatment 1 and kept constant for other treatments for simplicity.
γ (1)	0.15	Parameter γ represents the fraction of the total energy derived from biological decomposition of the substrate that is spent on heating the compost. The energy derived from biological decomposition is also utilized by bacteria and spent on water evaporation. This fraction was estimated by fitting the model to the experimental data from Yu [2007].
μ $(Pa \cdot hr)$	5.075e-9	The air viscosity in general depends on the temperature. We chose a constant value which corresponds to $18°C$ for simplicity.

Table 4.2: Parameter values that are kept constant for all treatments.

Parameter	Treatment				Comments
	1	2	3	4	
Φ_0 (%)	44.5	52.1	57.1	64.5	Initial air-filled porosity values were measured for all treatments.
ρ_0 (kg/m^3)	630	558.1	520.1	466.2	Initial bulk density values were measured for all treatments.
λ $(\frac{J}{kg\text{-}K})$	3600	3400	3200	3000	The heat capacity of the composting material was modified from Haug [1993]. It decreases as more wood chips are added to the compost, because the heat capacity of wood is less than the heat capacity of other components. The value of the heat capacity for each treatment was estimated by fitting the model to the data from Yu [2007].
$S_0(x)$ (kg/m^3)	0.1044· $\rho(x)$	0.1008· $\rho(x)$	0.0972· $\rho(x)$	0.0936· $\rho(x)$	The value for the initial substrate availability was estimated by excluding the 76% water content, assuming the biodegradability to be 50%, and excluding the wood chips content. Wood chips were considered inert and composed 13, 16, 19, and 22 percent of the substrate for Treatment 1, 2, 3, and 4, respectively.
C $(1/m^2)$	6.25e6	2.04e7	4e7	1.03e8	The Kozeny-Carman constant was estimated for each treatment by fitting the model to the experimental data from Yu [2007] focusing mainly on the air flow data.
D (m^2/hr)	0.0011	0.0008	0.0007	0.0004	The values for the thermal diffusivity of compost have been modified from Haug [1993]. Thermal diffusivity of compost decreases as it becomes more porous. The value for each treatment was obtained by fitting the model to the data from Yu [2007].

Table 4.3: Parameter values that varied for different treatments.

4.3 Simulation Results

In this section, we present and discuss the results of the numerical simulations and their agreement with experimental data. The numerical solutions of the equations were found using the PDE module of COMSOL 4.0a, a finite element software developed by Comsol Inc. [2011]. COMSOL is generally used for multiphysics simulations using built-in equations, however, the software exposes its solvers through the PDE module which allows for entering custom equations directly.

In Sections 4.3.1-4.3.4, the temperature data and the model's predictions for the temperature are compared for all four treatments. In Section 4.3.5, we compare the model's predictions of the air flow with the measured values. The temperature data is presented at six locations in the vessel, which are denoted Position 0, 1, .., 5. Position 0 corresponds to the bottom of the vessel, and Position 5 to the top. In treatments 2 and 3, there is a lag in temperature increase when the temperature reaches approximately 45 $^{\circ}C$. This lag occurs due to a switch in the population of microorganisms from mesophiles (optimal temperatures are below 45 $^{\circ}C$) to thermophiles (optimal temperatures are above 45 $^{\circ}C$). As our model does not include the microorganisms, it does not simulate this lag.

We note that initially the model was fitted to the data from Treatment 3, and then only a small number of parameters from the obtained set was varied to reflect changing substrate composition in the other treatments. Therefore, the model's fit with the data is best for Treatment 3. The treatments are presented below starting with Treatment 1 for ease of comparison. The parameters that were changed for different treatments are listed in Table 4.3.

4.3.1 Treatment 1

The first treatment corresponds to the lowest initial air-filled porosity value $\Phi_0 = 44.5\%$ and the highest initial density $\rho_0 = 630\ kg/m^3$. The experimental temperature profiles along with their trend lines are presented in Figure 4.3, and the model's predictions for temperature are shown in Figure 4.4. The maximum temperature for this treatment is between $45^{\circ}C$ and $50^{\circ}C$, which is the lowest of all treatments. The time required

for decomposition in this treatment is the longest, as concluded from comparing the temperature data for all four treatments.

The model is able to predict the peak temperature as well as estimate the time required for the decomposition. The model also successfully predicts which point in the vessel has the highest temperature (0.3 m from the bottom, shown in blue on the graphs). The data demonstrates that the bottom point of the vessel has a slightly higher temperature than the top (Position 0 and Position 5 on the graphs). The model's predictions, however, demonstrate that the temperature at the bottom is slightly cooler, probably because of the cool air entering the vessel at the bottom.

4.3.2 Treatment 2

The initial air-filled porosity and density values for the second treatment are $\Phi_0 = 52.1\%$ and $\rho_0 = 558.1\ kg/m^3$. The experimental temperature profiles are presented in Figure 4.5, and the model's predictions for temperature are shown in Figure 4.6. In this treatment, more wood chips had been added to the composting material which increased its air-filled porosity and decreased its density as compared to Treatment 1. The peak temperature reached is slightly less than $60°C$, which is higher than the maximum temperature for Treatment 1. The time required for decomposition in this case is shorter than for Treatment 1.

The model correctly predicts the maximum temperature value, and there is good agreement between the times at which the peak temperature is achieved. The point in the vessel that has the highest temperature (0.3 m from the bottom) is also predicted by the model. The lowest temperature point, according to the data, is at the top of the vessel. However, similarly to the Treatment 1 prediction, the model shows that the lowest temperature point is located at the bottom of the vessel, where the cool air enters the compost.

4.3.3 Treatment 3

Treatment 3 has higher initial air-filled porosity and lower initial density than Treatment 2. The initial air-filled porosity value for this treatment is $\Phi_0 = 57.1\%$, and the initial density is $\rho_0 = 520.1\ kg/m^3$. The experimental temperature profiles are presented in Figure 4.7, and the model's predictions for temperature are shown in Figure 4.8. The peak temperature value is just above $60°C$, which is higher than the peak temperature for Treatment 2. The peak temperature for this treatment is achieved faster than in Treatment 2.

This treatment was used to initially fit the model to data, and the model's prediction for this case has the best agreement with the experimental data among all treatments. The model successfully predicts the minimum and maximum temperatures and their locations, temperature distribution within the pile, and the approximate time when the peak temperature is reached.

4.3.4 Treatment 4

Treatment 4 has the highest initial air-filled porosity and the lowest initial density value of all treatments. The initial air-filled porosity for this treatment is $\Phi_0 = 64.5\%$, and the initial density is $\rho_0 = 466.2\ kg/m^3$. The experimental temperature profiles for this treatment are shown in Figure 4.9, and the model's predictions for temperature are presented in Figure 4.10. The peak temperature in this treatment is the highest (between $65°C$ and $70°C$) among all treatments, and it is achieved in a very short time (approximately 50 hours) compared to other cases.

Note that in the experiment, after approximately 90 hours, the substrate was removed, mixed, and returned to the vessel. This causes a jump in data shown in Figure 4.9. We can see that before the mixing, the 3 bottom points show the lowest temperature values around $40°C$, and the points at 0.3 and 0.5 meters are the hottest (above $65°C$). The temperature at 0.4 m is significantly cooler (between $55°C$ and $60°C$). This distribution is inconsistent with the distributions observed in the first three treatments, where there was a hot area around the middle of the vessel and the temperature gradually decreased

from that area towards the edges. After mixing, the hottest point switches to 0.4 m and the temperature distribution becomes more typical.

The model successfully predicts the maximum and minimum temperature values and demonstrates a significant decrease in time required for decomposition compared to other treatments, which follows the overall trend observed throughout the treatments.

4.3.5 Model Predictions for Air Flow and Oxygen Concentration

During the course of the experiments, the air flow was measured at the inlet and at the outlet of the vessel (see Figure 4.1). The outlet air flow measured was consistently larger than the inlet flow, because of the release of carbon dioxide and other gases. In our model, the air flow at the inlet and at the outlet are the same, as the model does not account for the release of gases, and also assumes incompressibility of air. Therefore, we compare our model's predictions with the inlet air flow data.

The measured maximum air flow rate increases from the lowest air-filled porosity in Treatment 1 to the highest air-filled porosity value in Treatment 4. The model demonstrates the same trend (see Figure 4.11). The model's predictions of the maximum air flow rates are compared to the measured inlet flow rates in Table 4.4. As the air flow rate depends strongly on the permeability, the good agreement between our model's predictions of the air flow and the data confirms that the permeability values chosen are approximately correct.

The predicted values of the oxygen concentration sampled in the middle of the vessel (0.25 m from the bottom) are shown in Figure 4.12 for the four treatments. The oxygen concentration drops to a very low value within the first hour for all treatments, and then gradually recovers to the ambient oxygen concentration value. The oxygen recovery is fastest for Treatment 4 and slowest for Treatment 1.

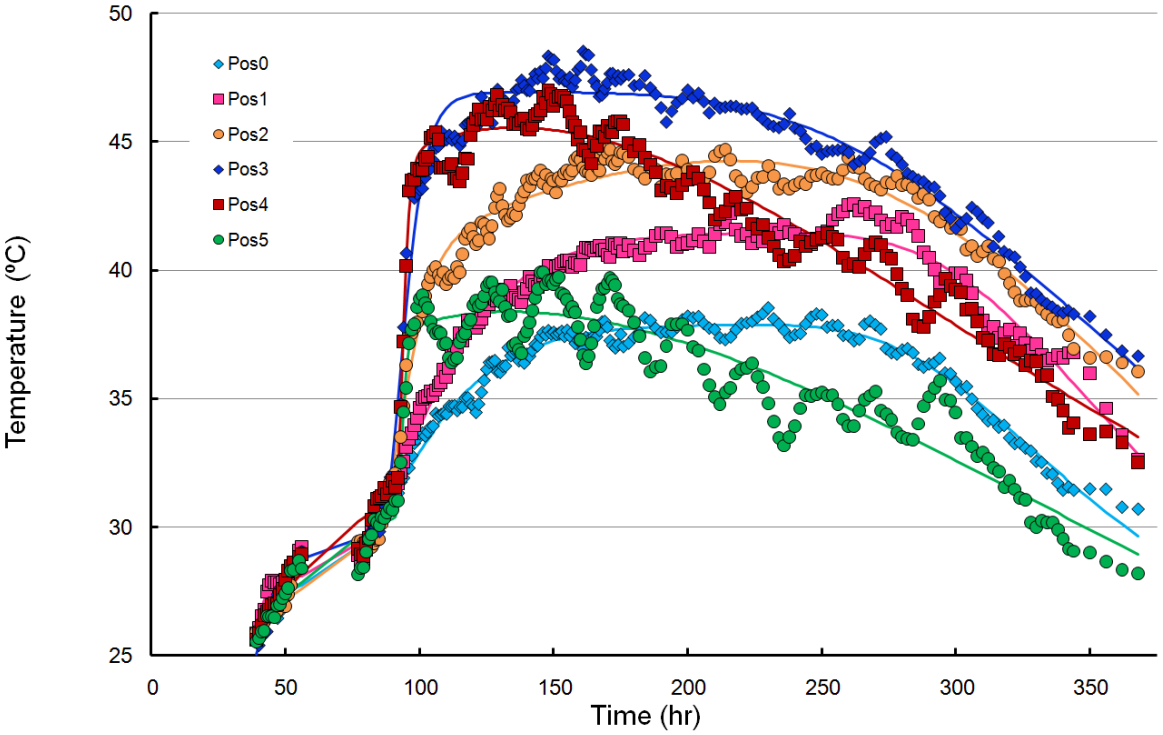

Figure 4.3: Experimental temperature profiles for Treatment 1.

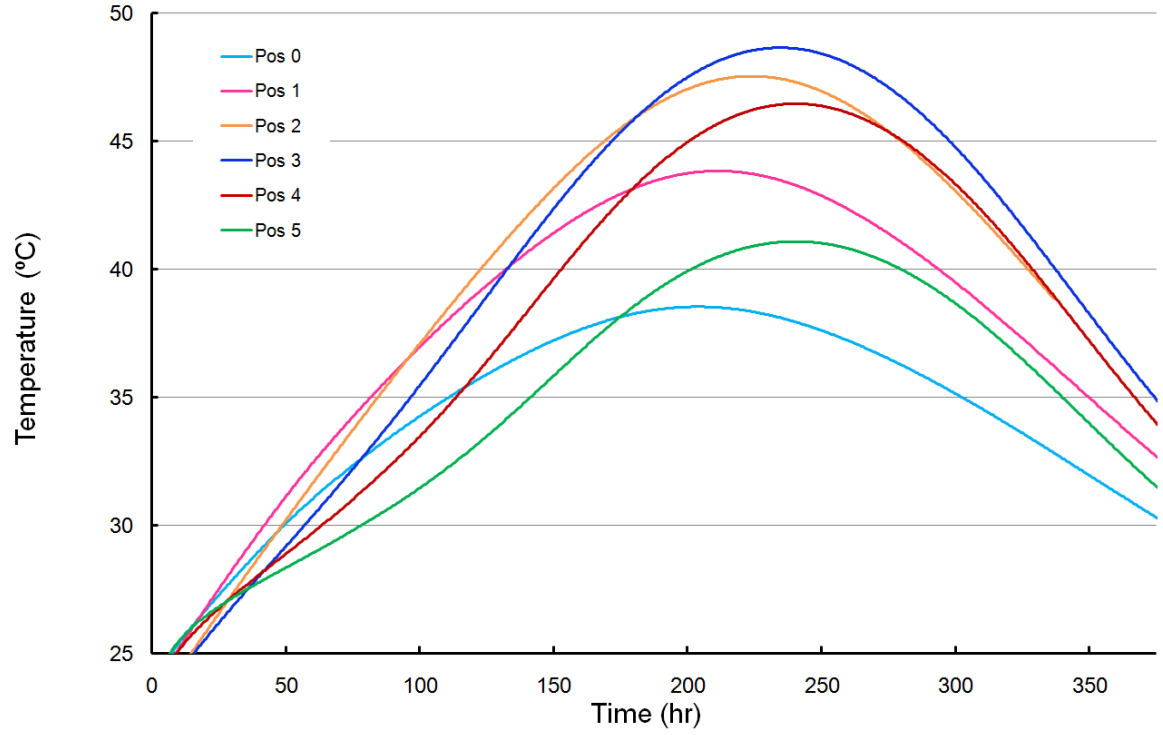

Figure 4.4: Predicted temperature profiles for Treatment 1.

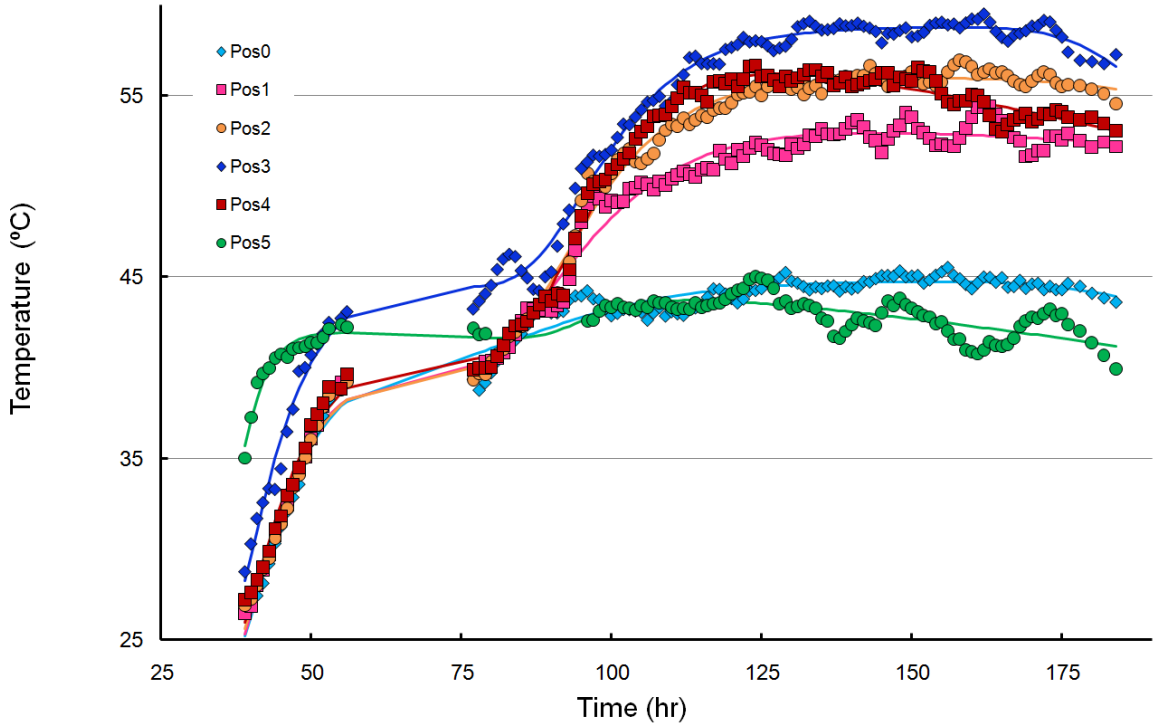

Figure 4.5: Experimental temperature profiles for Treatment 2.

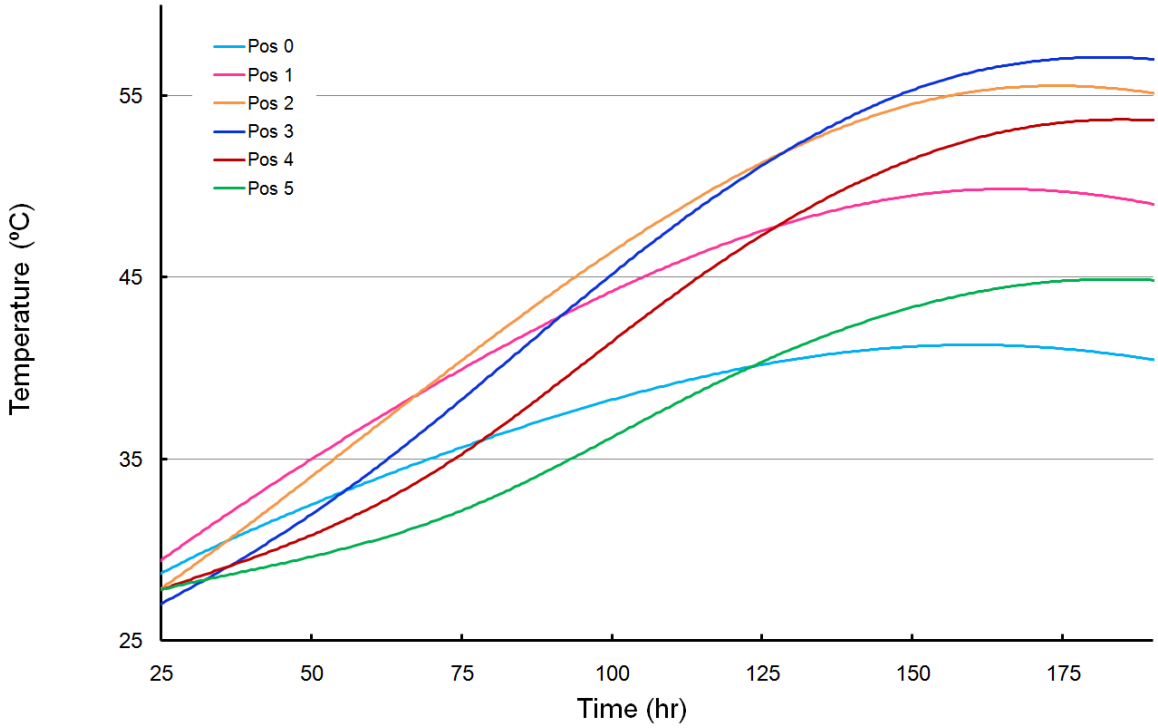

Figure 4.6: Predicted temperature profiles for Treatment 2.

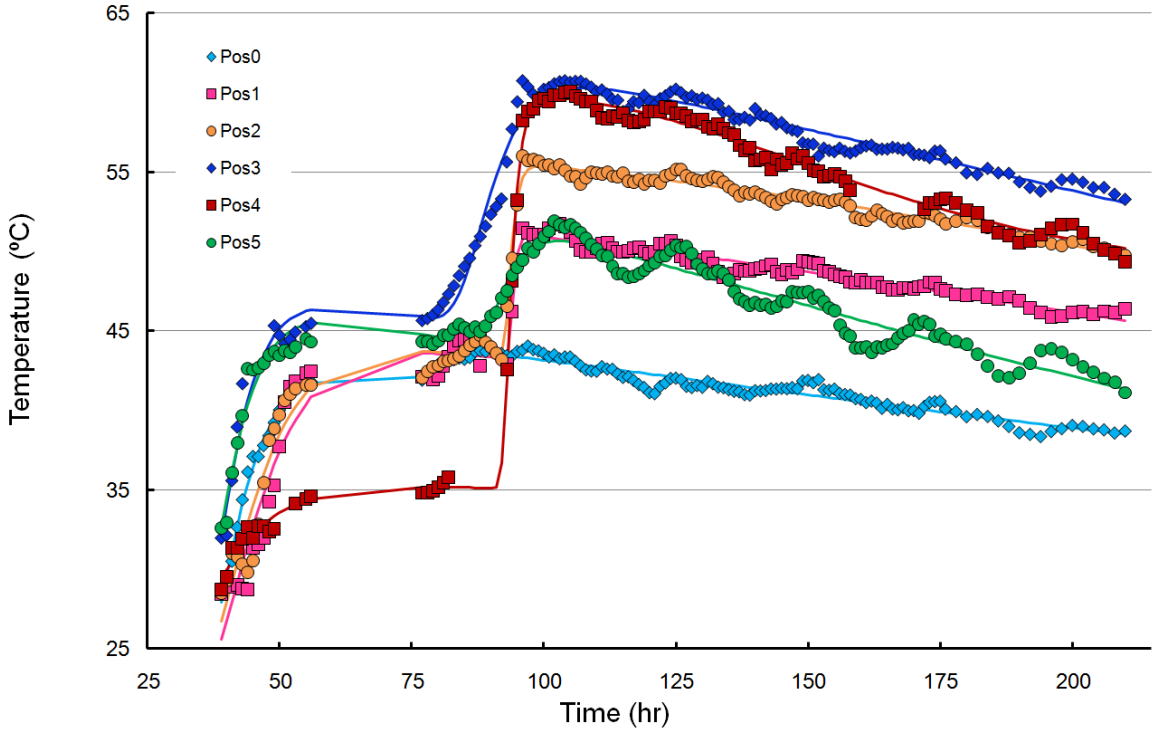

Figure 4.7: Experimental temperature profiles for Treatment 3.

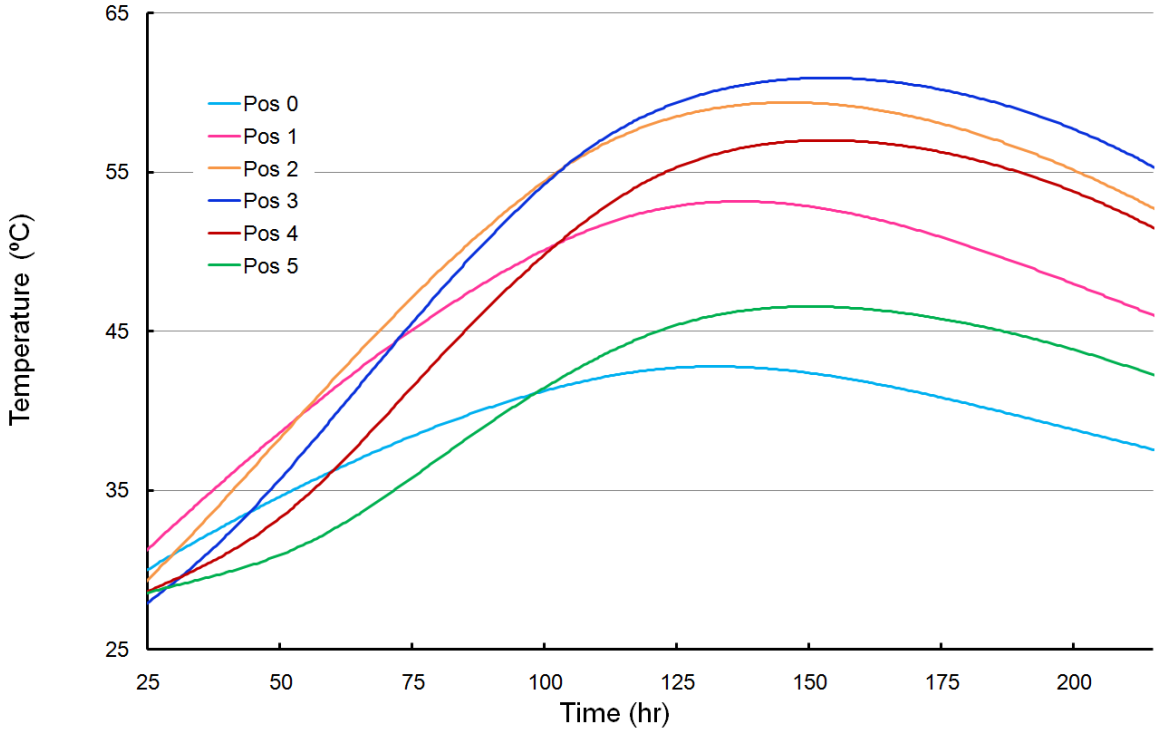

Figure 4.8: Predicted temperature profiles for Treatment 3.

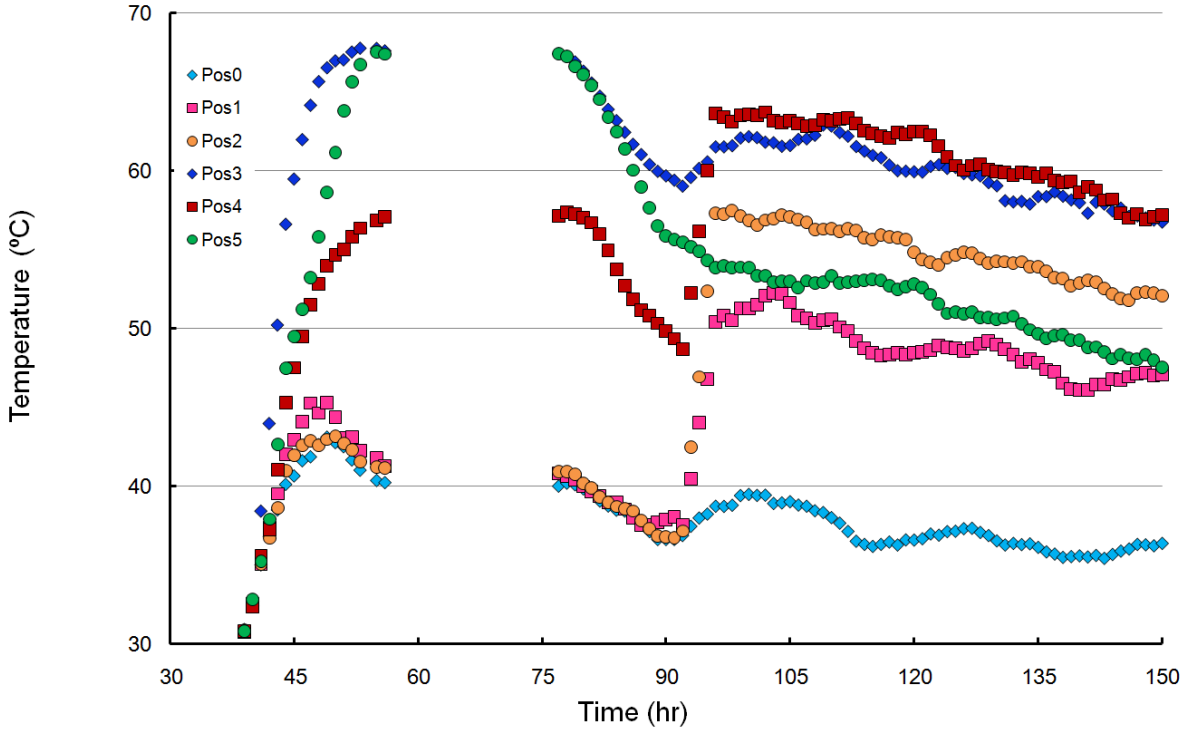

Figure 4.9: Experimental temperature profiles for Treatment 4.

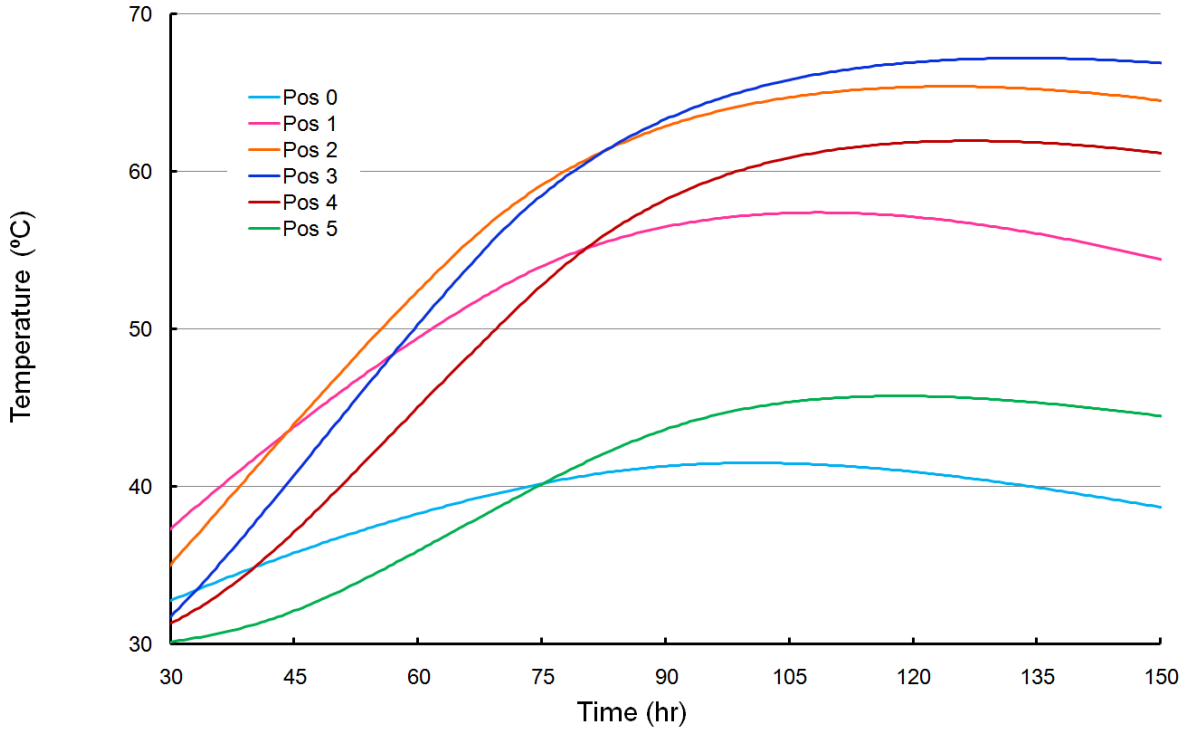

Figure 4.10: Predicted temperature profiles for Treatment 4.

	Treatment 1	Treatment 2	Treatment 3	Treatment 4
Max. Air Flow Measured	8.55	9.18	9.67	10.46
Max. Air Flow Predicted	7.94	8.95	9.56	10.88

Table 4.4: Measured and predicted maximum inlet air flow rate (L/min) for the four treatments.

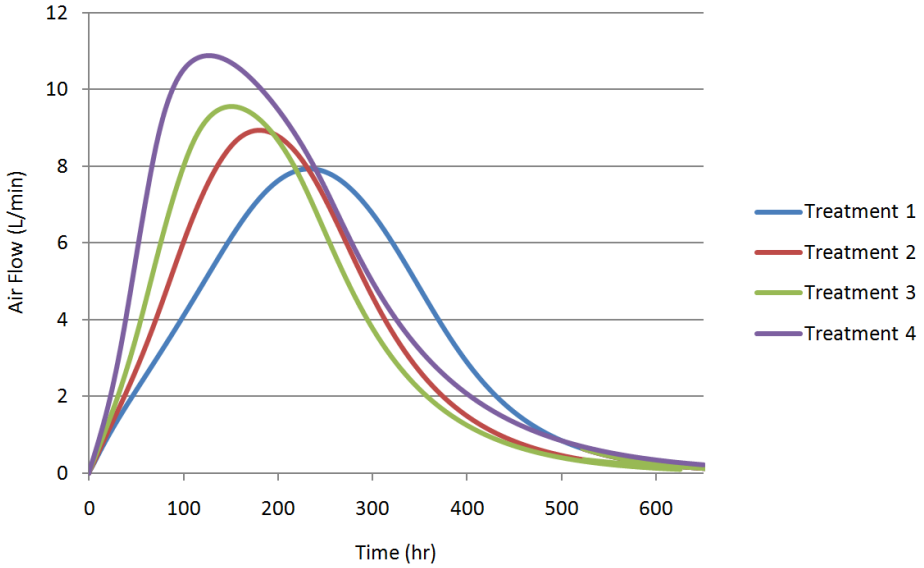

Figure 4.11: Air flow prediction for the four treatments.

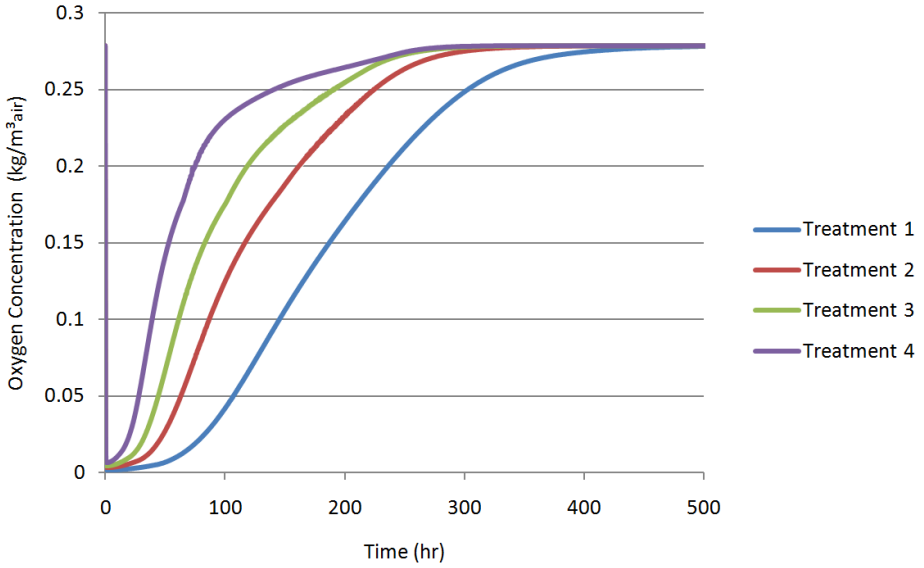

Figure 4.12: Oxygen concentration prediction at the middle of the vessel.

5 Modeling Windrows

In this chapter, we apply the parameters obtained in Chapter 4 to simulate windrow composting. We use the parameter set determined for Treatment 4. Parameter sets for other treatments correspond to lower initial air-filled porosity and permeability values, and we have observed that windrows do not heat up to temperatures above $40°C$ when parameters for treatments 1-3 are used. Low permeability values do not allow for a strong air flow to develop and effectively replenish the oxygen in the pile, and small oxygen concentrations limit the reaction.

In Section 5.1, we describe how our model is applied to simulate a two-dimensional cross-section of a windrow, and present boundary and initial conditions used in the simulations. In Section 5.2, we discuss in detail a simulation of a windrow with height $H = 1\ m$. We examine the temperature, oxygen concentration, available substrate, and pressure profiles at different times during the composting process, as well as the air flow patterns within the windrow. In Section 5.3, we investigate the effects of varying the size of the windrow on the composting process, and compare the average decomposition speeds for piles of different sizes. In Section 5.4, we apply our model to simulate air floor technology. We look at the effects of varying the size of the windrow for windrows placed on an air floor and compare the average decomposition speeds for piles placed on the ground and for piles placed on an air floor. We present the air flow patterns, and also the temperature, oxygen concentration, available substrate, and pressure profiles at different times for an aerated windrow with $H = 1\ m$.

5.1 Model Setup

We consider a two-dimensional cross-section of a windrow Ω. As shown in Figure 5.1, it is a right isosceles triangle. The cross-section has a height $H\ (m)$, the sides are denoted A and B, and the bottom of the cross-section is denoted C.

The initial conditions for our simulations are as follows:

$$\begin{aligned} T(0,\vec{x}) =& T_{amb}, \quad T_{air}(0,\vec{x}) = T_{amb}, \quad O_2(0,\vec{x}) = O_2^{amb}, \\ & S(0,\vec{x}) = S_0, \quad P(0,\vec{x}) = P_{atm}, \end{aligned} \tag{5.1}$$

where $T_{amb} = 20°C$ is the average ambient temperature, $O_2^{amb} = 0.2784\ kg/m^3_{air}$ is the ambient oxygen concentration, S_0 is the initial available substrate density, and $P_{atm} = 101325\ Pa$ is the standard atmospheric pressure.

On sides A and B of the windrow (see Figure 5.1), we apply Dirichlet boundary conditions for the temperature of the air T_{air}, pressure P, and oxygen concentration O_2:

$$T_{air}(t,\vec{x}) = T_{amb}, \quad P(t,\vec{x}) = P_{atm}, \quad O_2(t,\vec{x}) = O_2^{amb}, \quad \vec{x} \in A, B. \tag{5.2}$$

For the temperature T of the composting material, we apply the flux condition that represents Newton's law of cooling, as described previously in Section 4.2:

$$\frac{\partial T}{\partial \vec{n}}(t,\vec{x}) = -\frac{U}{\lambda \rho D}(T - T_{amb}), \quad \vec{x} \in A, B, \tag{5.3}$$

where $\vec{n}$ is an outward normal unit vector. For the available substrate S, a no-flux condition is used:

$$\frac{\partial S}{\partial \vec{n}}(t,\vec{x}) = 0, \quad \vec{x} \in A, B. \tag{5.4}$$

We have previously applied the same boundary conditions in Chapter 3 at the bottom and at the top of the experimental vessel.

On the bottom of the windrow, labeled C in Figure 5.1, we prescribe a Dirichlet boundary condition for temperature T and temperature of the air T_{air}:

$$T(t,\vec{x}) = T_{air}(t,\vec{x}) = T_{amb}, \quad x \in C. \tag{5.5}$$

The ground is assumed to be a perfect conductor and therefore will always keep the ambient temperature. Because the ground is impermeable, a no-flux condition is used

for the other three variables of the model:

$$\frac{\partial O_2}{\partial \vec{n}}(t,\vec{x}) = \frac{\partial S}{\partial \vec{n}}(t,\vec{x}) = \frac{\partial P}{\partial \vec{n}}(t,\vec{x}) = 0, \quad \vec{x} \in C. \tag{5.6}$$

Compaction was accounted for as described in Chapters 3-4. Sample distributions of air-filled porosity, density, permeability, and initial substrate availability for a windrow with height $H = 1\ m$ are presented in Figure 5.2. We can see that the strongest compaction effect occurs in the center at the bottom of the pile, where stress is the largest.

5.2 Sample Simulation of a Windrow

In this section, we consider in detail a simulation of a windrow with height $H = 1\ m$. We look at how maximum temperature, average oxygen concentration, and substrate availability in the compost pile vary with time. We also present the spatial profiles of temperature, oxygen concentration, substrate availability, pressure, and air flow patterns at several different times during the composting process.

The maximum temperature of the windrow as a function of time is presented in Figure 5.3. The maximum temperature reaches its peak value after approximately 30 days. This time scale is consistent with experimental observations from Stutzenberger et al. [1970].

The average oxygen concentration is shown in Figure 5.4. It first drops to its lowest value of 0.05 kg/m^3_{air} within the first hour, and then gradually recovers to the ambient oxygen concentration value.

To show the depletion of substrate S, we calculate the *fraction of available substrate* S relative to the substrate at the beginning of the process S_0 averaged over the domain:

$$s(t) = \frac{1}{H^2}\int_\Omega \frac{S}{S_0} d\Omega, \tag{5.7}$$

where Ω is the cross-section of the windrow and $H^2 = |\Omega|$ is the total area of Ω (see Figure 5.1). The graph of $s(t)$ is shown in Figure 5.5. We can see that the total substrate reaches zero at approximately the same time as when the peak temperature is achieved. The detailed substrate profiles at different times are shown in Figure 5.8 and will be

discussed later.

The temperature (T) profiles of the windrow after 200, 400, 600, and 800 hours of composting are presented in Figure 5.6. At the beginning of the process, the high temperature areas are located near the sides of the pile, where the oxygen concentration is higher than in the middle of the windrow. When the substrate on the sides is depleted, the biological decomposition moves to the middle.

At each time step, the volume flux of air $\vec{q}$ can be calculated using equation (3.16) at different points within the windrow, and therefore the air flow pattern can be plotted. Figure 5.7 shows the variation of the air flow pattern with time. The flow of air is strongest in the the areas with elevated temperatures. First, strong flow occurs near the edges of the windrow and then it gradually moves towards the middle.

The available substrate (S) profiles are shown in Figure 5.8. The profiles demonstrate the depletion of substrate taking place first near the edges of the pile, and then gradually moving towards the middle. The substrate in the center at the bottom of the pile degrades last, as this is the area of poor oxygen supply. Figure 5.5 demonstrates how the substrate is depleted over time.

The oxygen concentration (O_2) profiles are shown in Figure 5.9. By comparing Figures 5.8 and 5.9, we see that areas of low oxygen always correspond to the areas of high substrate availability, or the areas where the biological decomposition is taking place and therefore oxygen is consumed.

The differential pressure ($P - P_{atm}$) profiles presented in Figure 5.10 demonstrate a low pressure area on the bottom of the pile, which allows air to enter the windrow from the sides. This is consistent with experimental observations: Poulsen [2010] measured the pressure profiles in a windrow and noted that "in general, negative pressure is observed near the bottom while neutral or slightly positive pressures are observed in the central and upper parts of the pile". The magnitude of the differential pressure is on the order of 1 Pa, which is smaller than the values presented in [Poulsen, 2010] (reported differential pressure ranging from -20 Pa to 400 Pa). This could be due to different permeability values and, therefore, slower air flow.

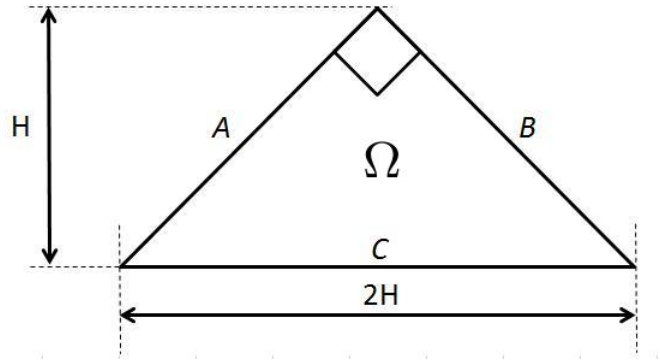

Figure 5.1: Diagram illustrating the cross-section of a windrow.

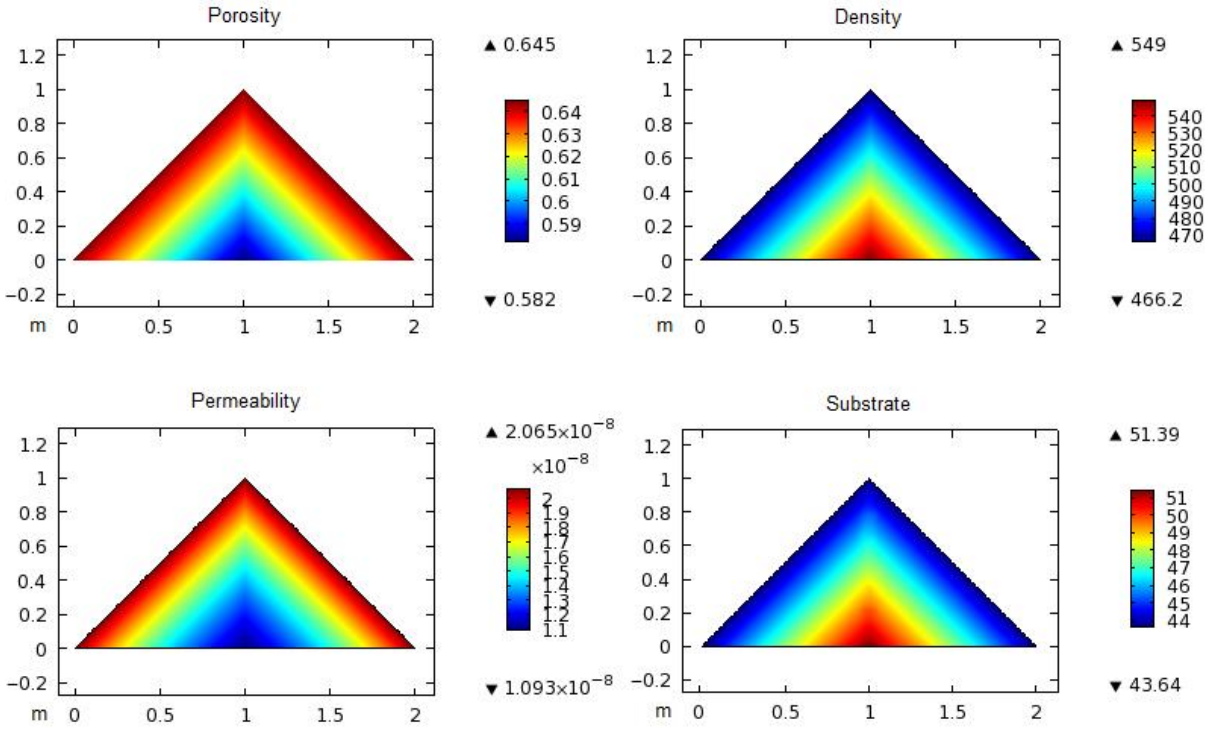

Figure 5.2: Effects of compaction on air-filled porosity (1), density (kg/m^3), permeability (m^2), and initial substrate density (kg/m^3) for a windrow with height $H = 1\ m$.

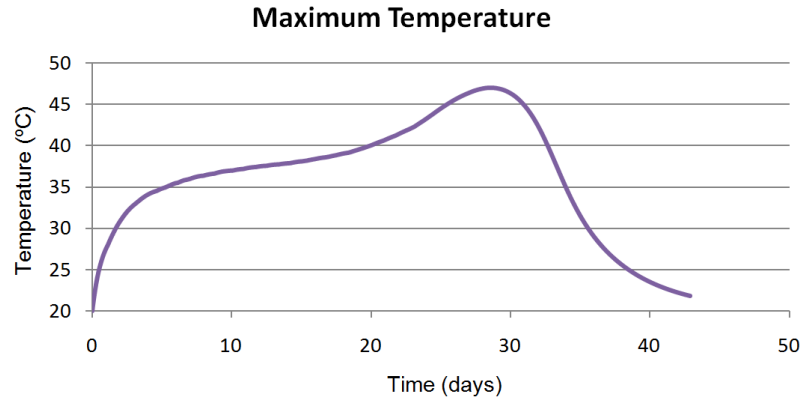

Figure 5.3: Maximum temperature variation in a windrow ($H = 1\ m$).

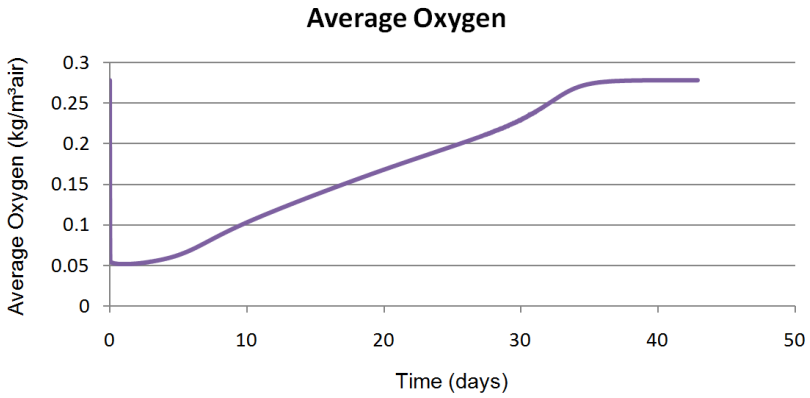

Figure 5.4: Average oxygen concentration variation in a windrow ($H = 1\ m$).

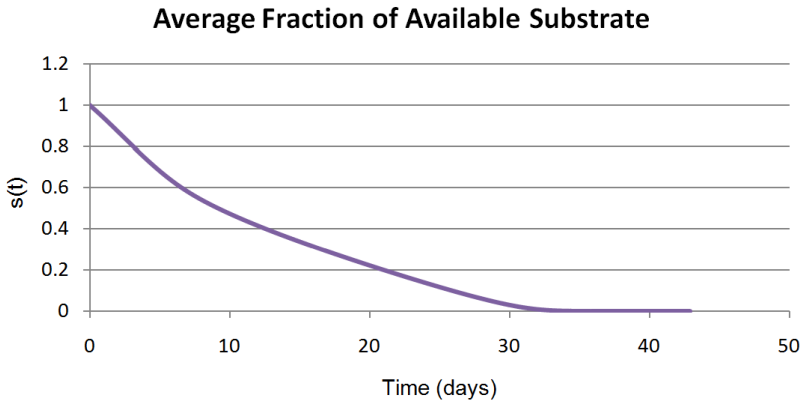

Figure 5.5: Average fraction of available substrate $s(t)$ variation in a windrow ($H = 1\ m$).

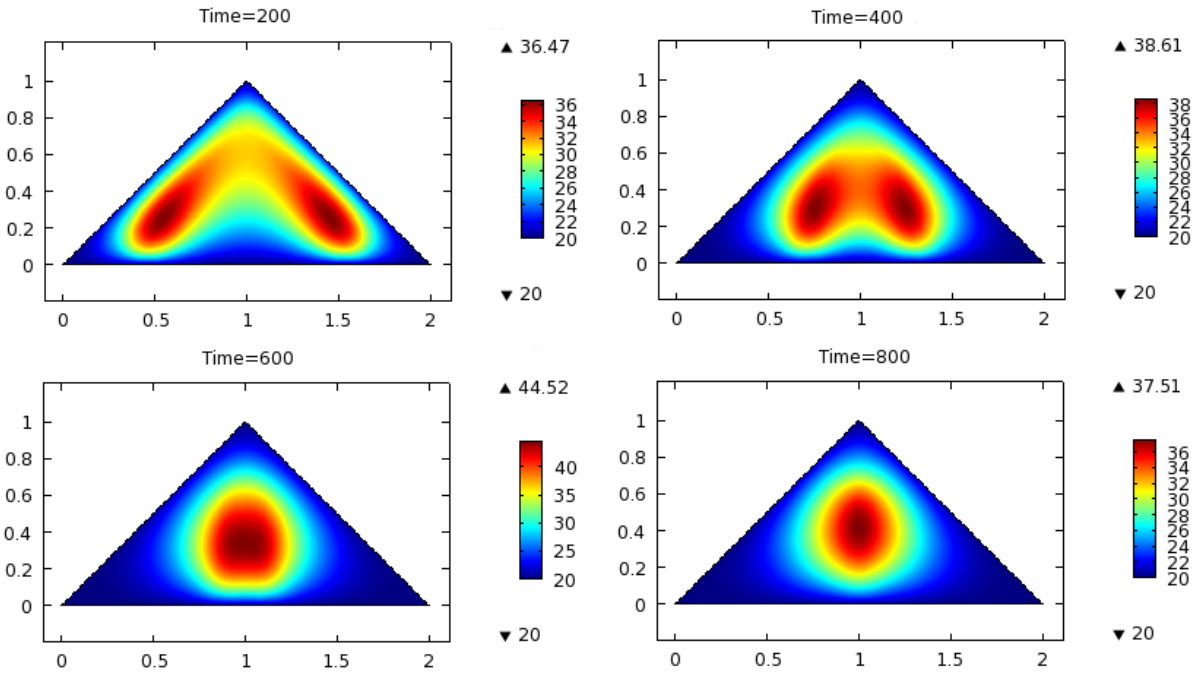

Figure 5.6: Temperature ($°C$) profiles in a windrow after 200, 400, 600, and 800 hours of composting ($H = 1\ m$).

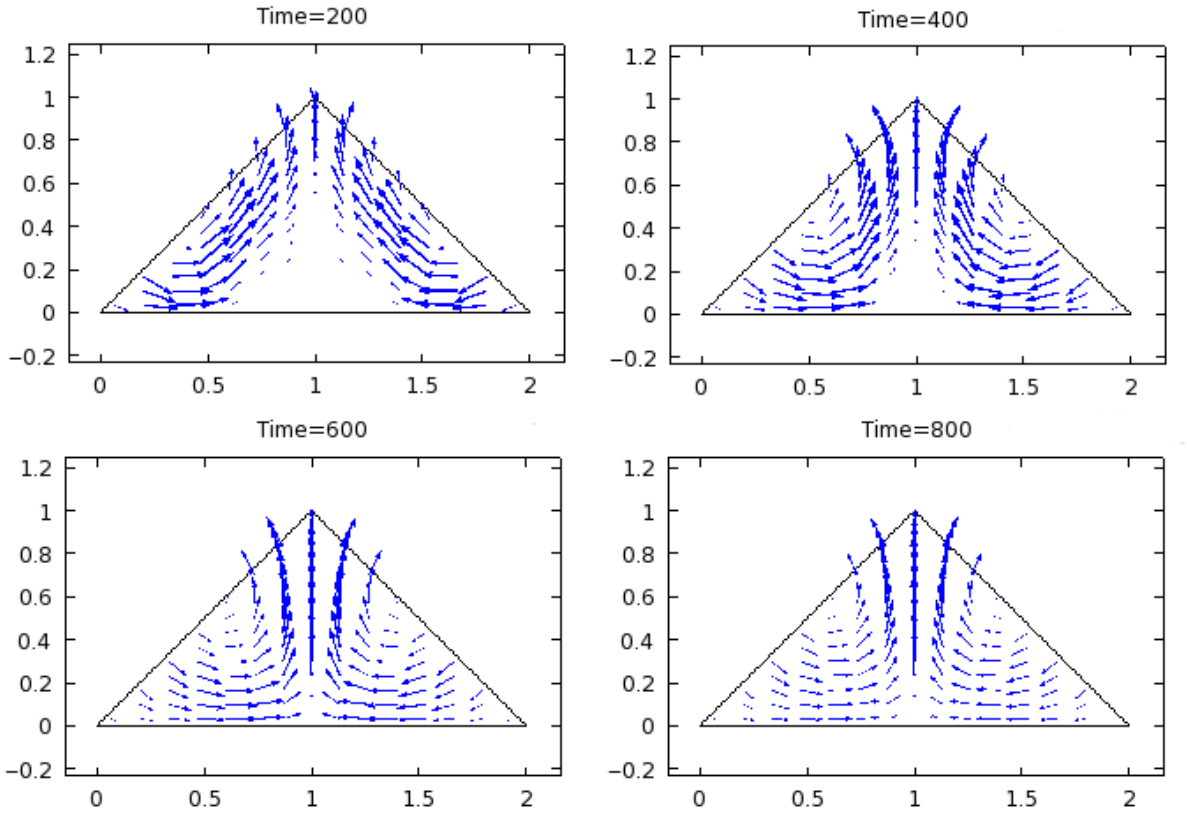

Figure 5.7: Air flow patterns in a windrow after 200, 400, 600, and 800 hours of composting ($H = 1\ m$).

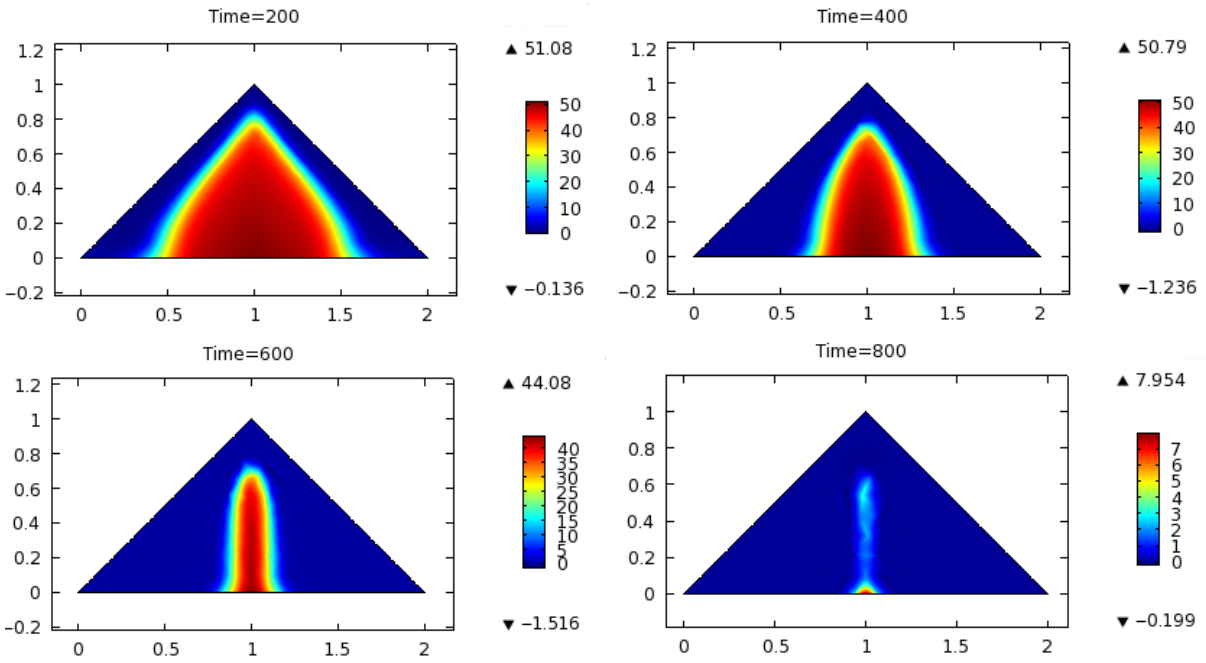

Figure 5.8: Available substrate S (kg/m^3) profiles in a windrow after 200, 400, 600, and 800 hours of composting $(H = 1\ m)$.

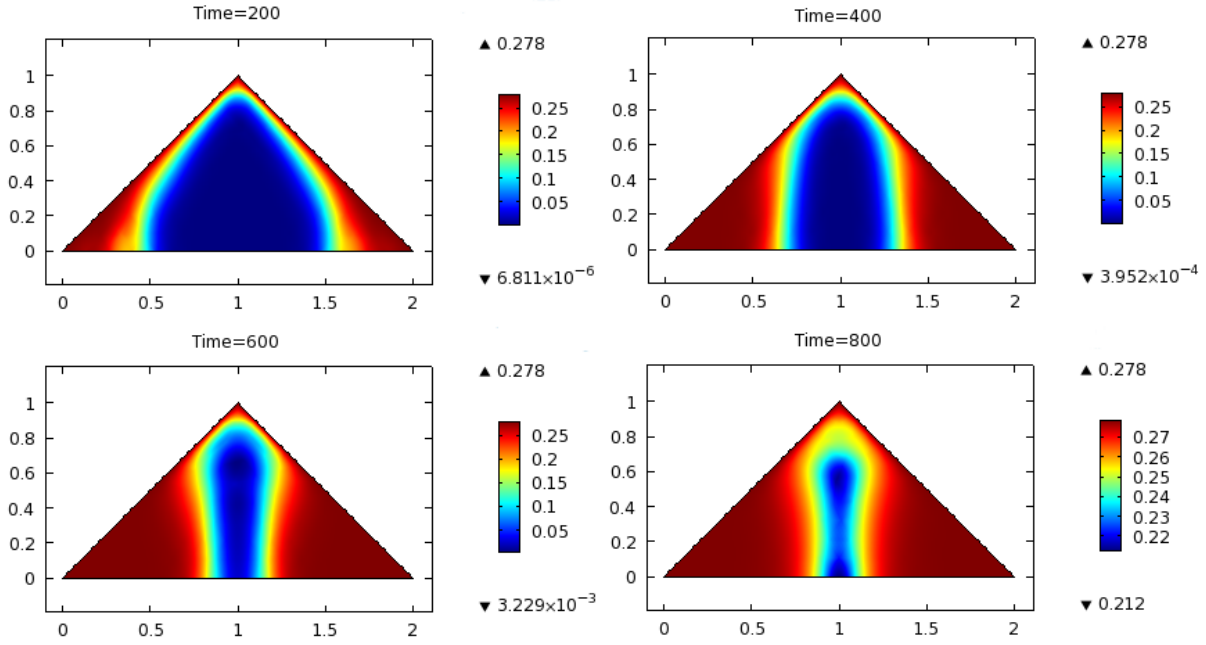

Figure 5.9: Oxygen concentration O_2 (kg/m^3_{air}) profiles in a windrow after 200, 400, 600, and 800 hours of composting $(H = 1\ m)$.

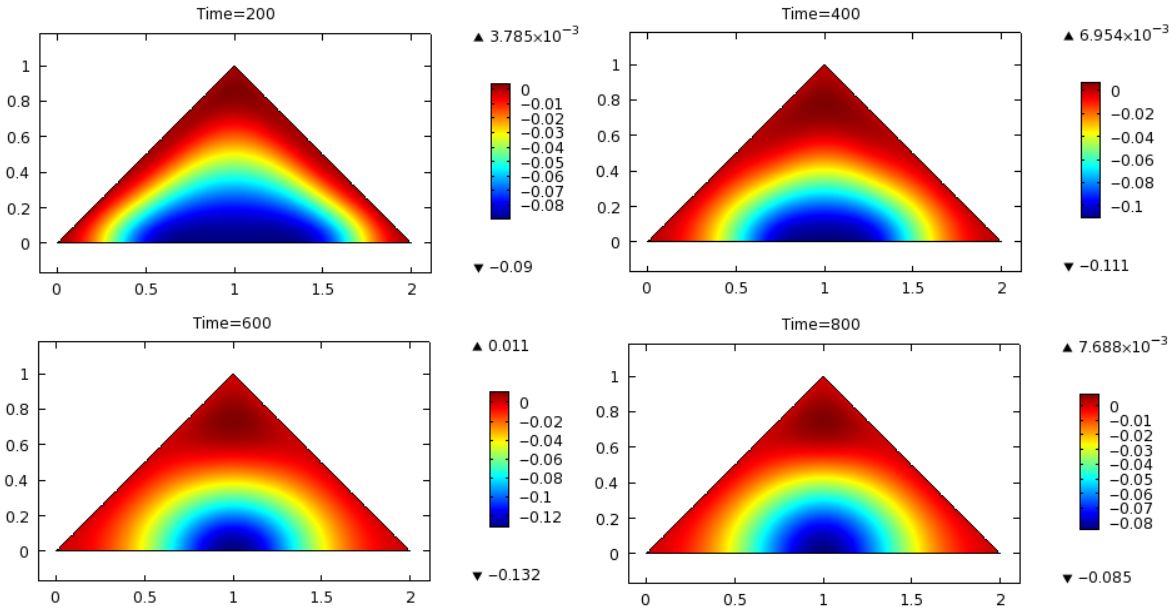

Figure 5.10: Differential pressure $(P - P_{atm})$ (Pa) profiles in a windrow after 200, 400, 600, and 800 hours of composting $(H = 1\ m)$.

5.3 Effects of Windrow Size

In this section, we investigate the effects of varying the size of the windrow on the composting process. We vary the height of the windrow H while keeping its relative shape constant (see Figure 5.1).

First, we plot the maximum temperature in the pile as a function of time for different pile sizes (see Figure 5.11). As the height of the pile increases, the peak temperature and the time required to achieve it increase. Larger piles are able to retain heat better than smaller piles, and therefore achieve higher temperatures.

The average oxygen concentrations in the pile for different pile sizes are presented in Figure 5.12. The average oxygen concentration initially drops to a very low value and then gradually recovers to the ambient oxygen concentration value. We can see that for large piles the recovery time is longer and the oxygen concentration initially drops to lower values than it does for smaller piles.

At each time step, we calculate $s(t)$, which is the fraction of available substrate S relative to the substrate at the beginning of the process S_0 averaged over the domain (see equation (5.7)). The graphs of $s(t)$ for different pile heights are presented in Figure 5.13. We can see that the larger the pile is, the more time is required for decomposition. To compare decomposition speeds for different pile sizes, we introduce the average decomposition speed v ($\frac{kg}{m\text{-}day}$). To do so, we first introduce t_{total} $(days)$, which is the total time required for $s(t)$ to decrease to 2%. To compute v, we divide the total initial amount of substrate by t_{total}:

$$v = \frac{\int_\Omega S_0 d\Omega}{t_{total}}, \tag{5.8}$$

where Ω is the cross-section of the pile. The obtained average decomposition velocities are plotted as a function of pile height in Figure 5.14. As the height of the pile increases from 0.5 m to 1.75 m, we observe a significant increase in the average decomposition speed. As the height increases above 1.75 m, the gain in the average decomposition speed becomes smaller. This demonstrates that as the pile height increases and its ability to retain heat improves, the average decomposition speed increases. However, for large piles, the

oxygen concentration limitations come into play and limit the increase of the speed of decomposition.

Intuitively, it is expected that to achieve high temperatures, the ratio between the surface area of the pile and its volume should be minimized to decrease the heat loss through the boundary. We test this hypothesis using our simulation results for different pile heights. As we are considering a two-dimensional cross-section of a windrow, the ratio between the surface area and the volume for our geometry is

$$\frac{\text{Surface Area}}{\text{Volume}} = \frac{\text{Boundary Length}}{\text{Cross-sectional Area}} = \frac{2\sqrt{2}H}{H^2} = \frac{2\sqrt{2}}{H}, \tag{5.9}$$

where $2\sqrt{2}H$ is the length of the exposed boundary of the cross-section, and H^2 is its area. We calculate these ratios for different pile sizes and plot the corresponding peak temperatures. The results are presented in Figure 5.15. The figure shows that as the ratio $\frac{Surface\ Area}{Volume}$ increases, the peak temperature decreases, which confirms the hypothesis.

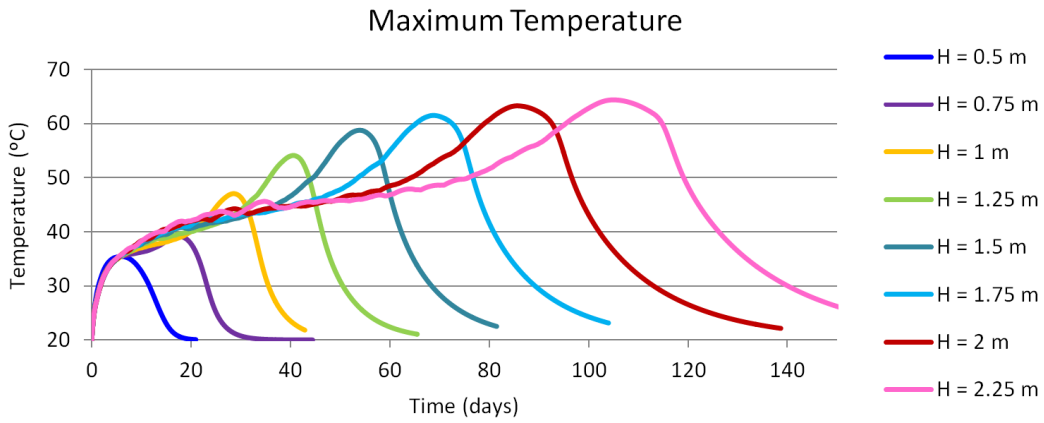

Figure 5.11: Maximum temperature variation in windrows of different sizes.

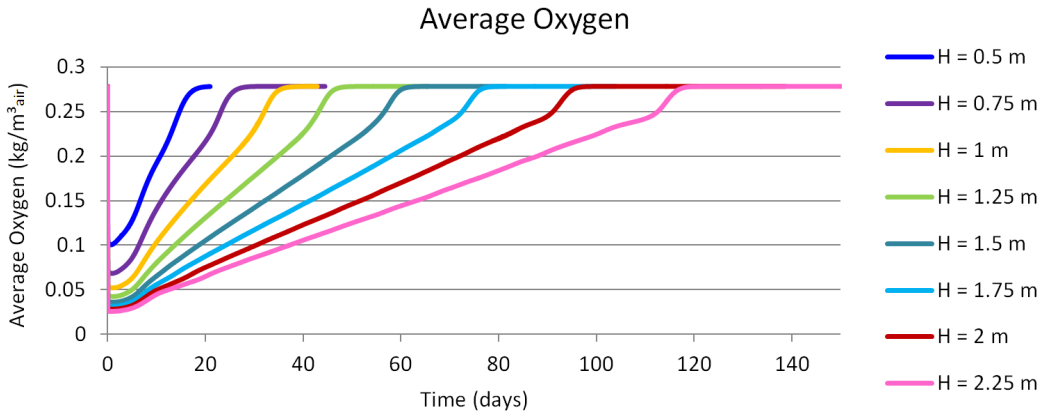

Figure 5.12: Average oxygen concentration variation in windrows of different sizes.

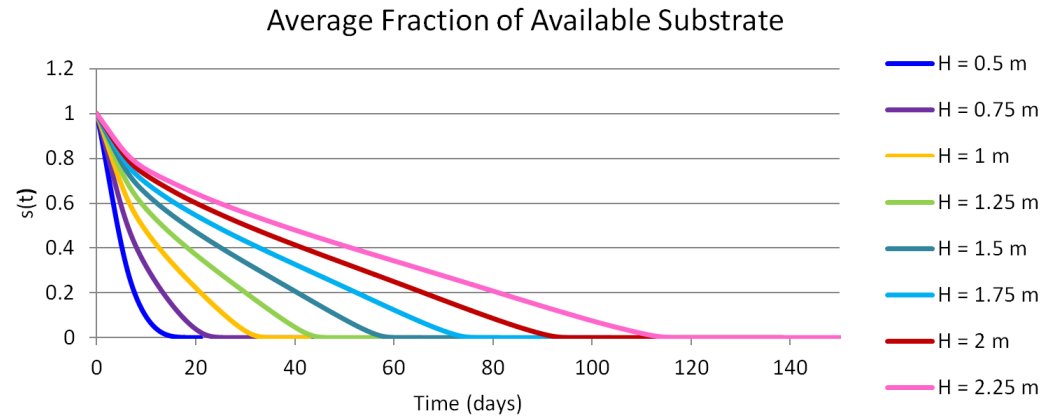

Figure 5.13: Average fraction of available substrate $s(t)$ variation in windrows of different sizes.

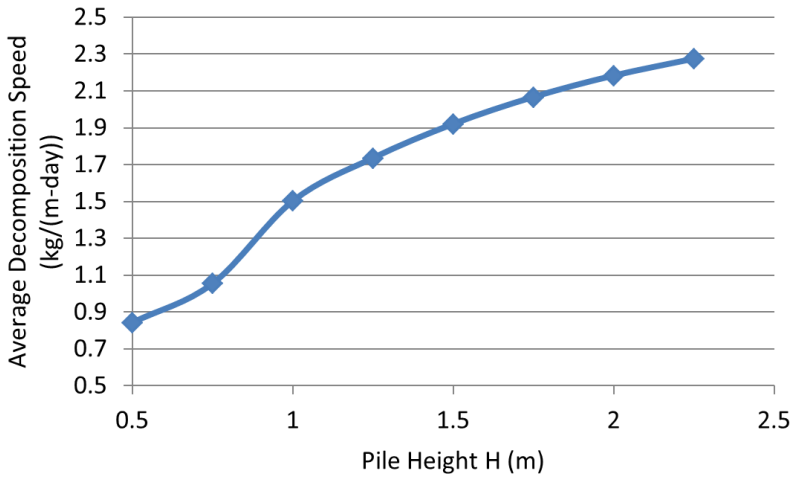

Figure 5.14: Average decomposition speed plotted as a function of pile height.

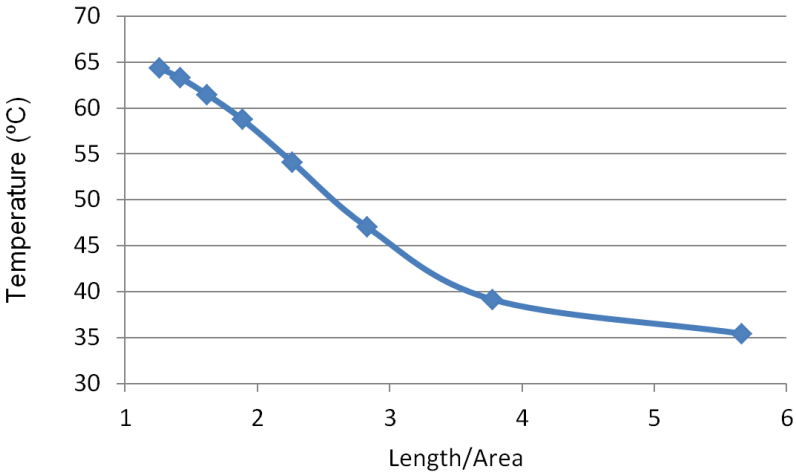

Figure 5.15: Peak temperature in the pile plotted as a function of the surface area to volume or length to area ratio.

5.4 Modeling Air Floor

In this section, we use our model to study how using air floor technology affects the composting process. An air floor is a concrete floor with pipes built under it. The pipes have small openings on the top which provide air to windrows (see Figure 5.16) and increase oxygen supply. To simulate the air floor, we use the same domain for our model as in the previous section, but modify the boundary conditions (see Figure 5.17). We assume there are 3 openings, each 2 cm wide, on the bottom of the windrow. The openings are located 0.5 m apart as shown in Figure 5.17. The boundary conditions along these openings are as follows:

$$T(t,\vec{x}) = T_{air}(t,\vec{x}) = T_{amb}, \quad O_2(t,\vec{x}) = O_2^{amb}, \quad P(t,\vec{x}) = P_{atm}, \quad \frac{\partial S}{\partial \vec{n}}(t,\vec{x}) = 0, \qquad (5.10)$$

where $\vec{x}$ belongs to intervals 3, 5, or 8 shown in Figure 5.17. The remaining sections of the bottom boundary maintain the boundary conditions defined by equations (5.5) and (5.6). The temperatures of compost and air are set to be equal to the ambient temperature, oxygen concentration is equal to the ambient oxygen concentration, pressure is equal to the atmospheric pressure, and there is no flux for the substrate. It should be noted that if air pumps are used, the pressure in the pipes will be higher than the atmospheric pressure, which can be easily incorporated into the model by changing the pressure value in equation (5.10).

The maximum temperature in a windrow as a function of time is plotted for different pile sizes in Figure 5.18. We can see that the maximum temperature is larger and the time required to achieve it is smaller for an aerated windrow than for a windrow of the same size placed on the ground (compare Figures 5.11 and 5.18). The average concentration in windrows of different sizes is presented in Figure 5.19. The average oxygen concentration recovers to the ambient value faster for aerated windrows (compare Figures 5.12 and 5.19). Figure 5.20 presents the average fraction of available substrate $s(t)$ (see equation (5.7)). Comparing Figures 5.13 and 5.20 shows that the time required for decomposition is smaller for aerated piles. Figure 5.21 compares the average decomposition speeds

for aerated piles and piles placed on the ground. A significant increase in the average decomposition speed is evident.

Figures 5.22 - 5.26 present the temperature profiles, air flow patterns, and available substrate, oxygen concentration, and pressure profiles of a windrow with height $H = 1\ m$ after 100, 200, 300, and 400 hours of composting. The temperature profiles qualitatively follow the same pattern as for the non-aerated windrow (compare with Figure 5.6). The elevated temperature areas first form near the sides of the windrow, and then join in the middle. The aerated windrow reaches higher temperatures than the windrow placed on the ground. The air flow patterns in Figure 5.23 show the air entering the compost from the openings on the bottom of the windrow.

The available substrate profiles are presented in Figure 5.24. The substrate is decomposed initially near the sides of the windrow where the oxygen concentration is high. We see that the oxygen provided by the openings allows the substrate on the bottom of the windrow to degrade faster than in a windrow with no aeration (compare with Figure 5.8). The oxygen concentration profiles (see Figure 5.25) demonstrate higher oxygen concentrations on the bottom of the pile than for the non-aerated windrow (compare with Figure 5.9). The pressure profiles presented in Figure 5.26 demonstrate similar behavior to pressure profiles of the non-aerated windrow (compare with Figure 5.10). A negative pressure area is formed on the bottom, with a slightly positive or zero pressure on the top. The openings on the bottom are seen on the profiles as points with zero, or atmospheric, pressure.

Figure 5.16: Air floor installation. Source: `http://www.transformcompostsystems.com`. Last accessed on September 15, 2011.

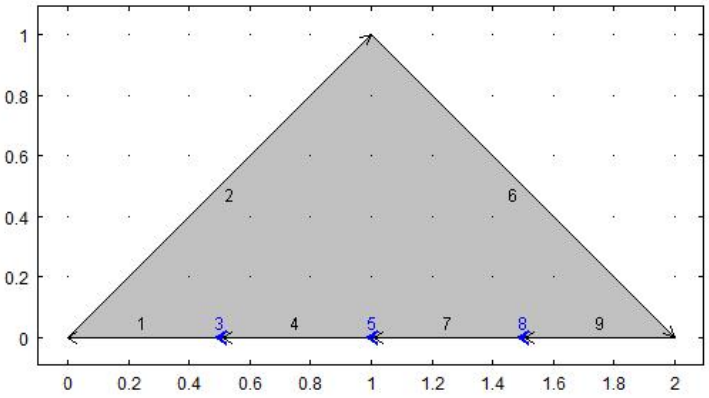

Figure 5.17: Cross-section of an aerated windrow with openings on the bottom.

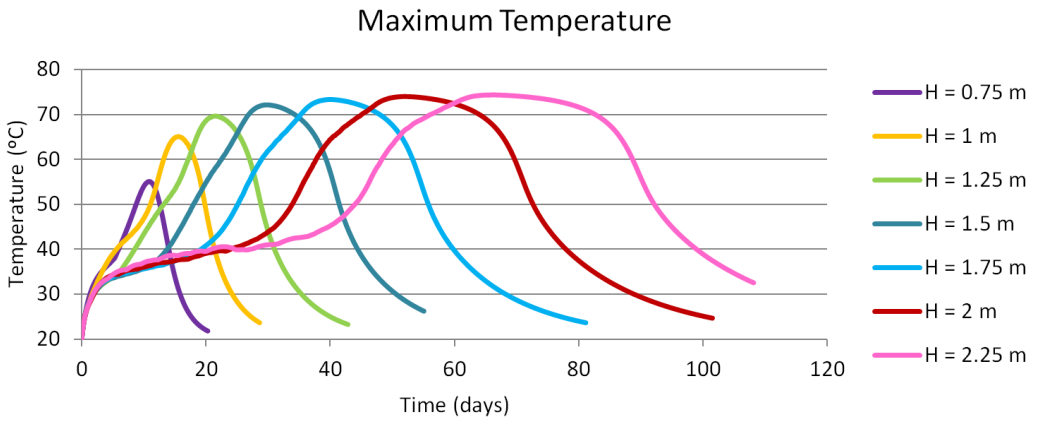

Figure 5.18: Maximum temperature variation in aerated windrows of different sizes.

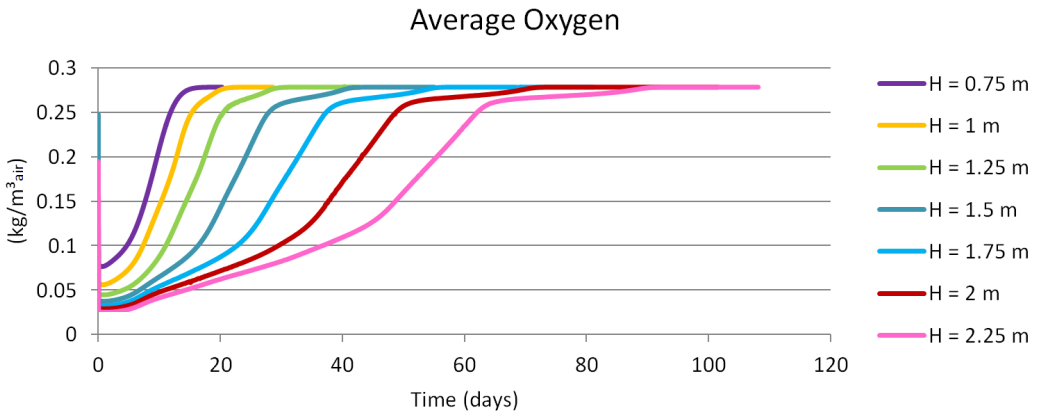

Figure 5.19: Average oxygen concentration variation in aerated windrows of different sizes.

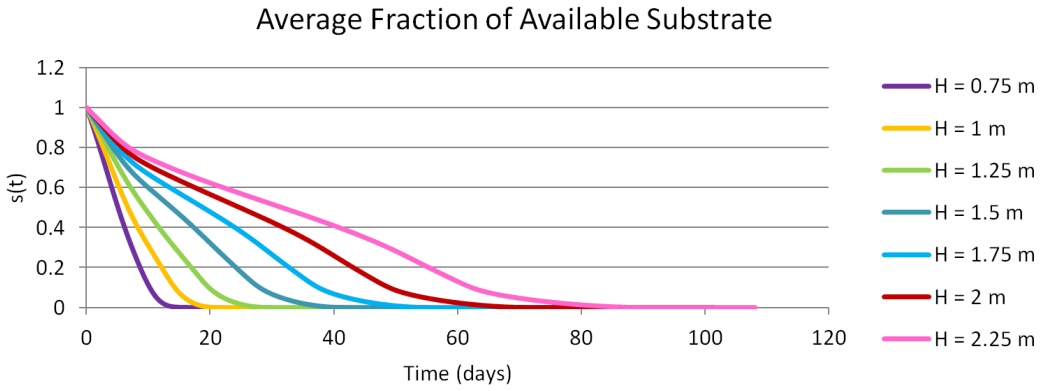

Figure 5.20: Average fraction of available substrate $s(t)$ variation in aerated windrows of different sizes.

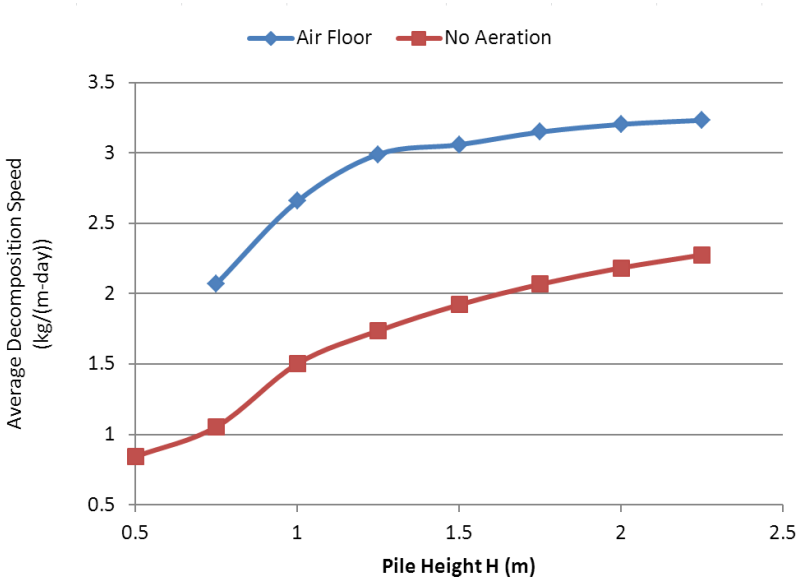

Figure 5.21: Average decomposition speed plotted as a function of pile height for aerated and non-aerated windrows.

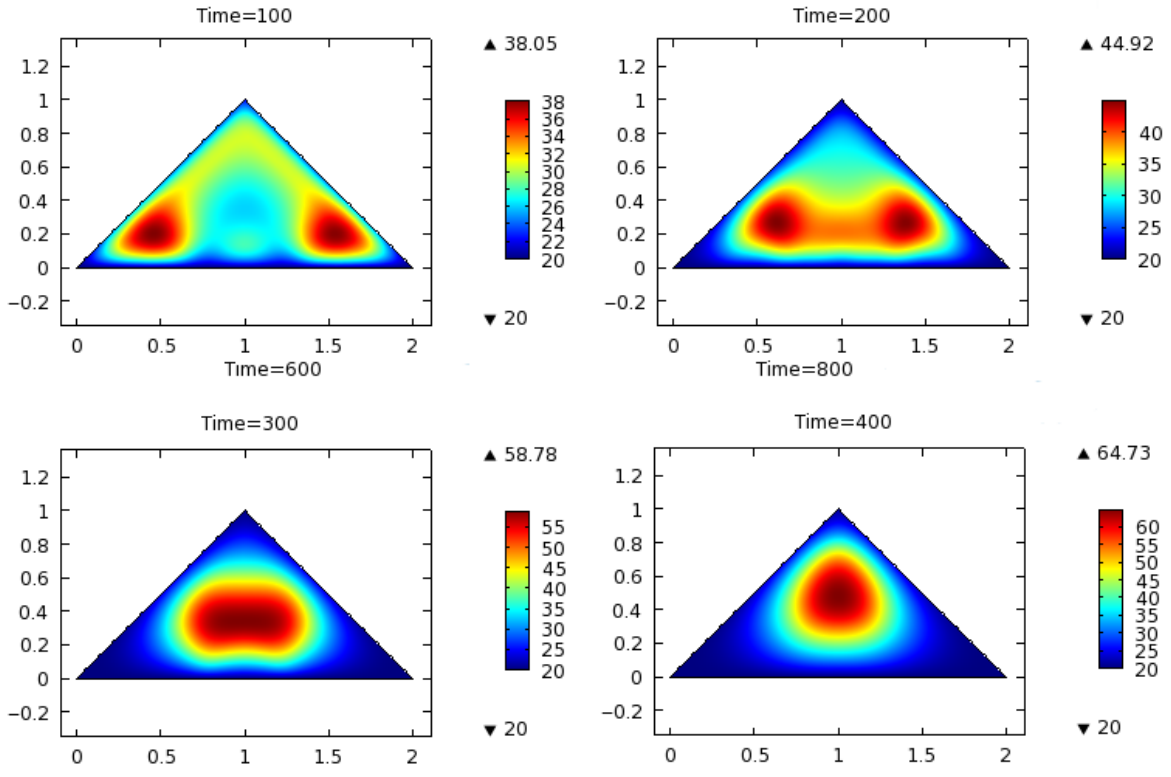

Figure 5.22: Temperature T ($°C$) profiles in an aerated windrow after 100, 200, 300, and 400 hours of composting ($H = 1\ m$).

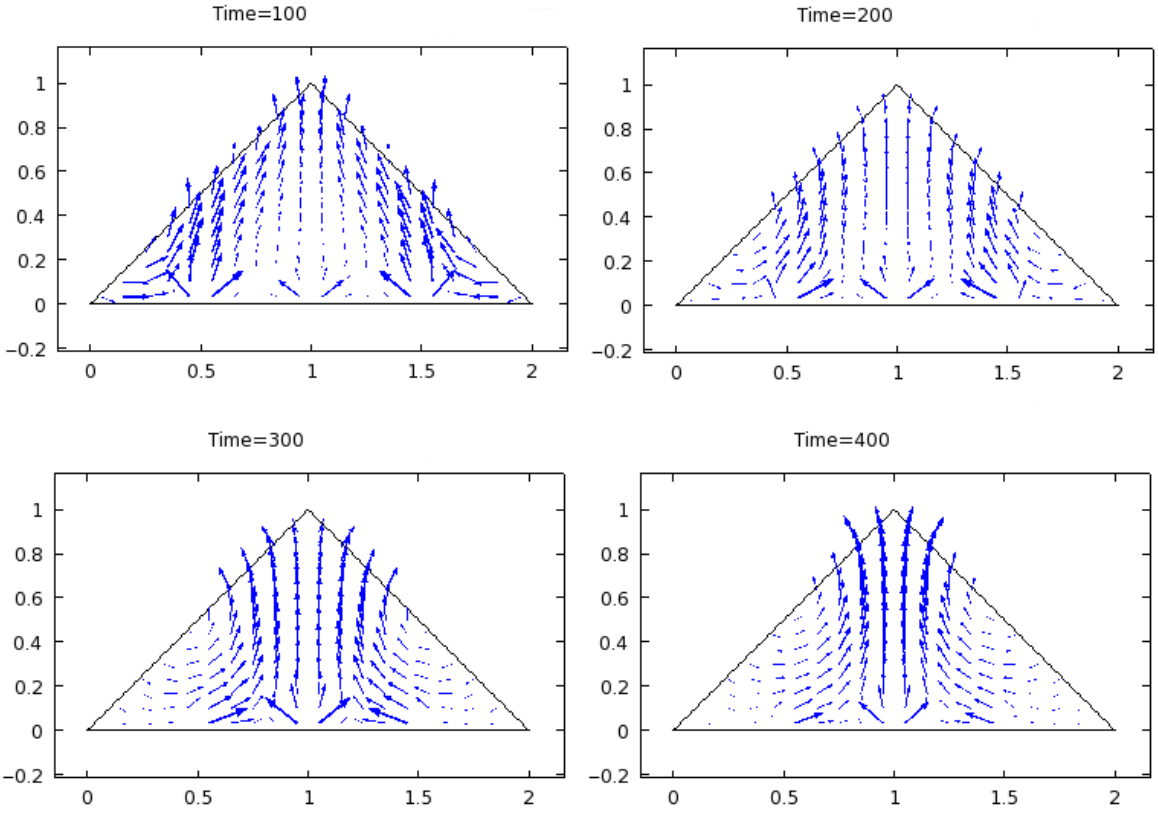

Figure 5.23: Air flow patterns in an aerated windrow after 100, 200, 300, and 400 hours of composting ($H = 1\ m$).

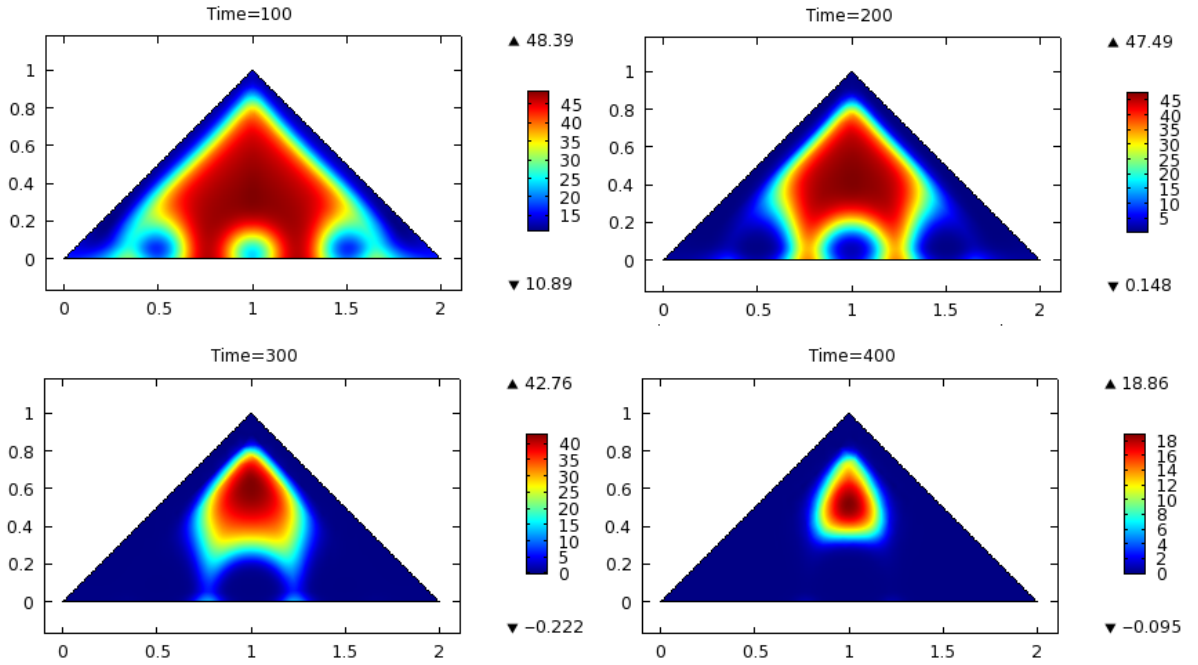

Figure 5.24: Available substrate S (kg/m^3) profiles in an aerated windrow after 100, 200, 300, and 400 hours of composting ($H = 1\ m$).

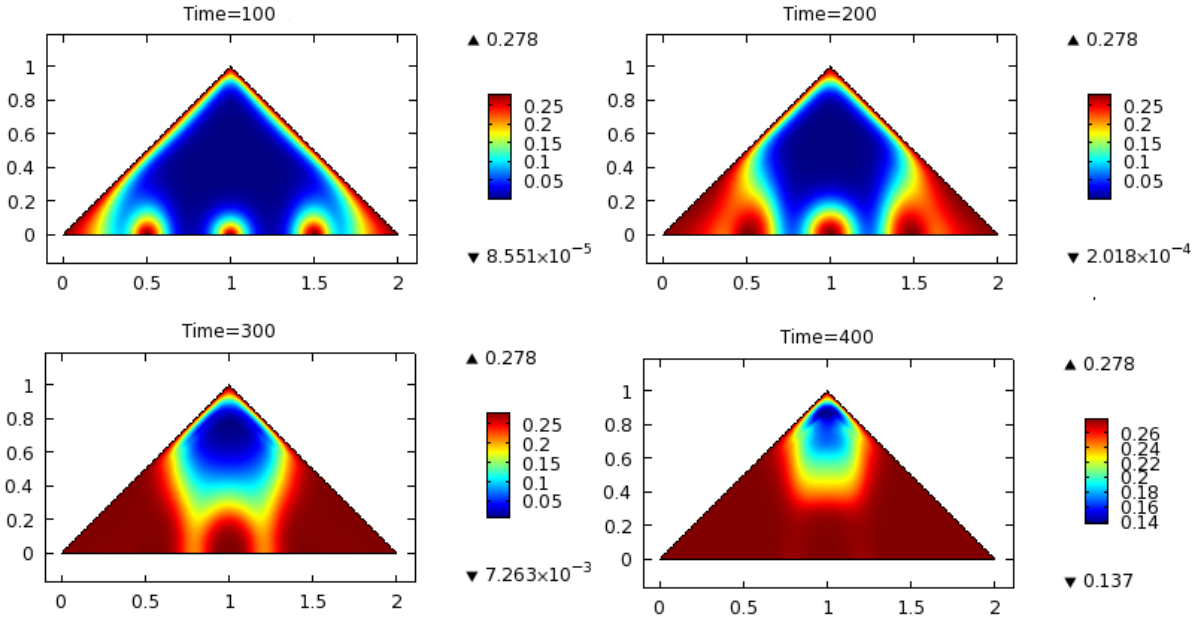

Figure 5.25: Oxygen concentration O_2 (kg/m^3_{air}) profiles in an aerated windrow after 100, 200, 300, and 400 hours of composting ($H = 1\ m$).

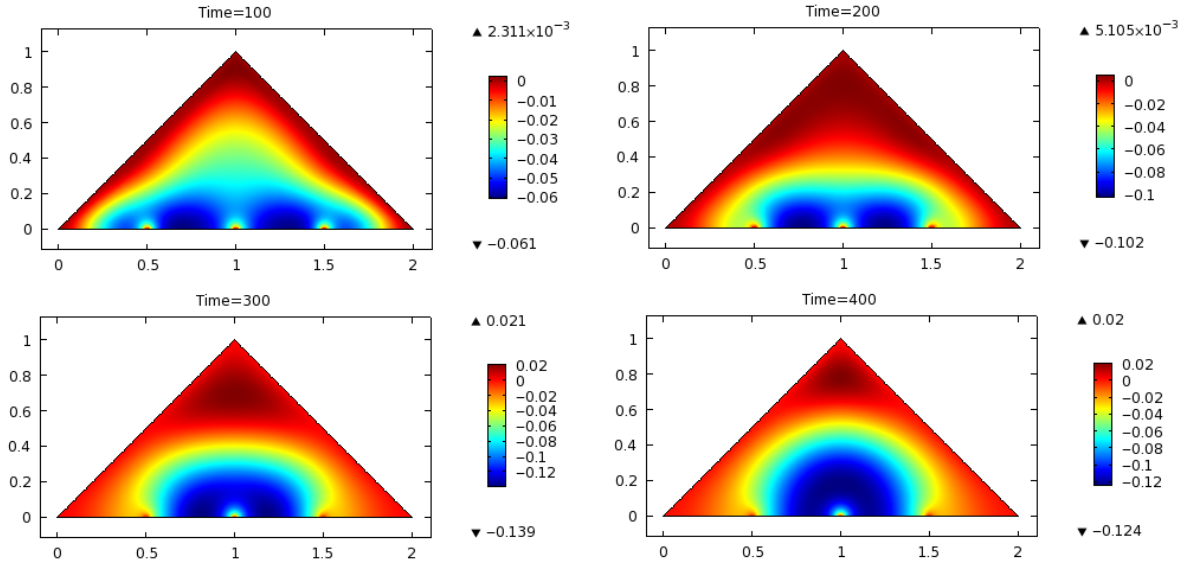

Figure 5.26: Differential pressure $(P - P_{atm})$ (Pa) profiles in an aerated windrow after 100, 200, 300, and 400 hours of composting $(H = 1\ m)$.

6 Discussion

6.1 Summary

In this thesis, a novel spatial mathematical model for the composting process was developed. In Chapter 2, we reviewed, to our best knowledge, all the existing spatial models for composting. The models described do not account for the consumption of organic matter and do not give a realistic prediction of the air flow patterns in a compost pile. Additionally, most models neglect the cooling of the composting material by passing air, and the models that do incorporate cooling use a simplified, prescribed air flow pattern. A realistic prediction of the air flow is important because buoyant flow of air is the main mechanism of oxygen supply in passively aerated compost piles [Haug, 1993].

In Chapter 3, we developed a model for composting which overcomes the limitations mentioned above. The model gives a realistic prediction of the air flow patterns, includes the cooling of the composting material by passing air, and accounts for substrate consumption, therefore examining the process from the beginning to the end of decomposition. A new way of incorporating cooling of the compost by passing air into the model was introduced. This was done by considering a new independent variable T_{air}, which allowed us to account for the cooling of the compost by passing air, as well as for a possible heating of the compost that may take place when warm air enters a cooler part of the compost pile. The existing models do not include temperature of air as a separate variable, and assume uniform cooling of the compost.

One of the important challenges in modeling compost is uncertainty in parameter values. While some of the required parameters have well-established values, other parameters, such as reaction rates and permeability, have wide ranges of reported values. Parameter values are also dependent on the specific substrate used. In Chapter 4, we validated our model using the experimental data from Yu [2007]. We fixed the parameters which have well-established values, and varied the parameters that have wide ranges of reported values in the literature to fit the experimental data. The model was fitted to four sets of data which corresponded to four experiments conducted for different ini-

tial air-filled porosity and density values. We obtained a good fit with the experimental data, successfully predicting the peak temperatures and the times at which the peak temperatures occurred.

In Chapter 5, we used the parameter values obtained in Chapter 4 to simulate windrow composting. Effects of varying the windrow size were explored for piles placed on the ground as well as for piles placed on an air floor. The model demonstrated the increase in peak temperature with increasing pile size, which agrees with general observations in the field. The average decomposition speed was computed for piles of various sizes. The speed increased as the pile size increased, and the gain in speed was smaller for larger piles, demonstrating that larger piles face oxygen limitations which reduce the increase in decomposition speed. In addition, the model was applied to windrows placed on an air floor. The model clearly showed an increase in peak temperature and a decrease of the total time required for decomposition for aerated piles compared to piles placed on the ground.

6.2 Future Work

Our model's predictions of substrate profiles in a windrow demonstrated that the substrate first degraded near the edges of the pile where the oxygen concentration was higher. In reality, the substrate on the edges of the pile degrades poorly because of low moisture values and low temperatures. In our simulations, the low temperatures on the edges did not significantly reduce the rate of decomposition because the temperature correction function ($f(T)$, in equation (3.12)) we used suggested that the temperature value of 20 $^{\circ}C$ (the ambient temperature in our simulations) does not pose significant limitations on the reaction rate. However, the predicted oxygen concentrations were very low and therefore limitations posed by oxygen dominated over the temperature limitations. As a future work direction, we suggest exploring different correction functions for temperature, such as the one used by Haug [1993], which propose more dramatic differences between composting rates at low and elevated temperatures (compare Figures 3.1 and 3.2). In addition, including moisture into the model would allow accounting for slower

composting in dry areas of the pile. Also, water vapor decreases the density of the air which contributes to its buoyancy, and therefore including water evaporation into the model would allow for a more accurate prediction of the air flow.

The experimental data from Yu [2007] demonstrates that the air flow at the inlet of the vessel was consistently smaller than the air flow at the outlet of the vessel. This increase in the air flow is mainly due to the carbon dioxide released in the biological decomposition reaction and the water vapor. Incorporating water vapor and carbon dioxide into the model would provide a more realistic prediction of the air flow by accounting for the change in the composition of air, filling the pores of the compost matrix.

In our model validation, we relied solely on temperature and air flow data. The model's predictions for other important variables such as pressure, oxygen concentration, and substrate availability could not be validated due to the lack of data. An important step in further improving the model would be to validate it against a more extensive set of data which includes oxygen and pressure profiles.

Many of the model parameters are dependent on the specific substrate, such as the stoichiometric coefficients, air-filled porosity, permeability, and maximum reaction rates. Using the parameter values specific to a particular substrate and then validating the model against the data obtained with this substrate would provide a more accurate feedback on the model's performance.

6.3 Conclusions

As noted earlier in Chapter 1, the spatial heterogeneity is an important feature of large-scale composting process which cannot be ignored by mathematical models. Therefore, we suggest that developing spatial models is an important direction in mathematical modeling of composting. The spatial model developed in this thesis overcomes the limitations of existing spatial models for composting. It accounts for the consumption of organic matter and considers the process from the beginning to the end of decomposition, gives a realistic prediction of the air flow pattern, includes the cooling of the compost by passing air, and incorporates the effects of compaction. The model can serve as a useful

tool in process optimization and facility design.

Bibliography

G. O. Brown, J. Garbrecht, and W. H. Hager. *Henry P.G. Darcy and other pioneers in hydraulics: Contributions in celebration of the 200th birthday of Henry Philibert Gaspard Darcy.* ASCE Publications, 2003.

K. Das and H. M. Keener. Moisture effect on compaction and permeability in composts. *Journal of Environmental Engineering*, 123(3):275–281, 1997.

S. M. Finger, R. T. Hatch, and T. M. Regan. Aerobic microbial growth in semisolid matrices: Heat and mass transfer limitation. *Biotechnology and Bioengineering*, 18(9):1193–1218, 1976.

W. B. Fulks, R. B. Guenther, and E. L. Roetman. Equations of motion and continuity for fluid flow in a porous medium. *Acta Mechanica*, 12(1–2):121–129, 1971.

S. Gajalakshmi and S. A. Abbasi. Solid waste management by composting: State of the art. *Critical Reviews in Environmental Science and Technology*, 38(5):311–400, 2008.

R. T. Haug. *The practical handbook of compost engineering.* Lewis Publishers, 1993.

Comsol Inc., November 2011. URL `http://www.comsol.com`.

Y. Liang, J. J. Leonard, J. J. Feddes, and W. B. McGill. A simulation model of ammonia volatilization in composting. *Transactions of the ASABE*, 47(5):1667–1680, 2004.

T. Luangwilai and H. S. Sidhu. Determining critical conditions for two dimensional compost piles with air flow via numerical simulations. *ANZIAM Journal*, 52:463–481, 2011.

T. Luangwilai, H. S. Sidhu, M. I. Nelson, and X. D. Chen. Modelling air flow and ambient temperature effects on the biological self-heating of compost piles. *Asia-Pacific Journal of Chemical Engineering*, 5(4):609–618, 2010.

I.G. Mason. Mathematical modelling of the composting process: A review. *Waste Management*, 26(1):3–21, 2006.

I.G. Mason. An evaluation of substrate degradation patterns in the composting process. Part 2: Temperature-corrected profiles. *Waste Management*, 28(10):1751–1765, 2008.

D. A. Nield and A. Bejan. *Convection in porous media.* Springer, 3 edition, 2006.

T. G. Poulsen. Temperature, pressure and air flow distribution in passively aerated compost piles. *Compost Science and Utilization*, 18(2):127–134, 2010.

T. L. Richard, L. P. Walker, and J. M. Gossett. Effects of oxygen on aerobic solid-state biodegradation kinetics. *Biotechnology Progress*, 22(1):60–69, 2006.

H. S. Sidhu, M. I. Nelson, and X. D. Chen. A simple spatial model for self-heating compost piles. *ANZIAM Journal*, 48:135–150, 2007a.

H. S. Sidhu, M. I. Nelson, T. Luangwilai, and X. D. Chen. Mathematical modelling of the self-heating process in compost piles. *Chemical Product and Process Modeling*, 2(2):8, 2007b.

D. P. Stombaugh and S. E. Nokes. Development of a biologically based aerobic composting simulation model. *Trans. ASAE*, 39(1):239–250, 1996.

F.J. Stutzenberger, A.J. Kaufman, and R.D. Lossin. Cellulolytic activity in municipal solid waste composting. *Canadian Journal of Microbiology*, 16(7):553–560, 1970.

S. Yu. *Heat and mass transfer in passively aerated compost.* PhD thesis, University of Alberta, 2007.

S. Yu, O.G. Clark, and J.J. Leonard. Airflow measurement in passively aerated compost. *Canadian Biosystems Engineering*, 47(6):39–45, 2005.

S. Yu, O. G. Clark, and J. J. Leonard. Estimation of vertical air flow in passively aerated compost in a cylindrical bioreactor. *Canadian Biosystems Engineering*, 50(6):29–35, 2008.